A Unified Performance Framework for Integrated Sensing-Communications based on KL-Divergence

Mohammad Al-Jarrah, *Member, IEEE*, Emad Alsusa, *Senior Member, IEEE,* and Christos Masouros, *Senior Member, IEEE,*

***Abstract*—The need for integrated sensing and communication (ISAC) services has significantly increased in the last few years. This integration imposes serious challenges such as joint system design, resource allocation, optimization, and analysis. Since sensing and telecommunication systems have different approaches for performance evaluation, introducing a unified performance measure which provides a perception about the quality of sensing and telecommunication is very beneficial. To this end, this paper provides performance analysis for ISAC systems based on the information theoretical framework of the Kullback-Leibler divergence (KLD). The considered system model consists of a multiple-input-multiple-output (MIMO) base-station (BS) providing ISAC services to multiple communication user equipments (CUEs) and targets (or sensing-served users). The KLD framework allows for a unified evaluation of the error rate performance of CUEs, and the detection performance of the targets. The relation between the detection capability for the targets and error rate of CUEs on one hand, and the proposed KLD on the other hand is illustrated analytically. Theoretical results corroborated by simulations show that the derived KLD is very accurate and can perfectly characterize both subsystems, namely the communication and radar subsystems.**

***Index Terms*—Integrated sensing and communication (ISAC), relative information, Kullback-Leibler distance, zero forcing (ZF) precoding, maximum ratio transmission (MRT) precoding, MIMO radar, multiple targets.**

I. Introduction

With the immensely successful deployment of fifth generation (5G) networks worldwide, many technologies, services and applications have been created. Examples for such technologies, include massive connectivity for internet-of-things (IoT) devices [1]–[3], autonomous or self-driving vehicles [4], and unmanned aerial vehicles (UAVs) [5], [6], which all rely on sensing and are subject to future developments. Therefore, sensing services such as detection, localization, tracking, navigation and environmental surveillance are expected to be supplied by network operators in the future to support these kinds of technologies. However, sensing services would add extra challenges due to limited network resources including spectrum, time and energy. Therefore integrating telecommunication services and sensing functionalities to optimize network resources have become an active research area for the past few years [7]–[13].

Generally speaking, remote sensing can be defined as the collection of measurements and data from the surroundings without physical contact with objects or the phenomena of interest [3], [14]. Sensing is used in a massive number of daily applications such as radar, LiDAR, IoT applications, electromagnetic sensing, underwater sensing, environmental sensing and monitoring, medical applications, global positioning systems (GPS), etc [1], [15]–[18]. Two main categories can be used to classify sensing systems, which are passive and active sensing. Whilst passive detectors rely on signals emitted from sources (e.g. infrared, the sunlight and smoke detectors) or reflected by objects as the case of cameras, energy is intentionally emitted from a source and the reflected or backscattered signals are detected and measured by sensors in the case of active type sensing. Examples for active sensing applications include conventional and multiple-input-multiple-output (MIMO) radars, LiDAR and sonar. In MIMO radars, the one intended in this work, multiple antennas are employed with digital receivers and waveform generators feeding the aperture. Unlike phased array radars in which the separation between the antenna elements is typically small, MIMO radars employ relatively widely separated antennas (e.g. $d \geq \lambda/2$, where d is the antenna separation and λ is the wavelength). Therefore, MIMO radars have the ability to integrate energy from different waveforms to obtain diversity gain which results in high resolution detection and localization capabilities [21]–[23].

On the other hand, in multi-user MIMO (MU-MIMO) communication systems, multiple beams can be transmitted from a base-station (BS) to serve a number of users with adequate data rates and quality-of-service (QoS). MIMO has become an integral element in wireless communications and has been adopted by several global standards and specifications such as 4G, 5G, IEEE 802.11n and WiMax, etc [24], [25]. More recently, massive MIMO BSs which are equipped with a large number of antennas, practically up to 256, are employed to provide connectivity to a significant number of users simultaneously. Moreover, by using a large number of antennas, inter-user interference can be efficiently eliminated due to the asymptotic orthogonality of the channels. Other significant advantages of massive MU-MIMO is achieving a huge capacity, enhancing the spectral efficiency without network densification, improving the energy efficiency, providing the ability to generate focused beams that feed small areas [24]–[27].

Evidently, there is a persistent evolution in wireless communication networks in general where BSs equipped with a large number of antennas play a main role in this evolution. Moreover, promoting the functionality of BSs to be able to provide sensing services in addition to their fundamental communication duties is unavoidable for efficient deployment of IoT and sensing systems. Therefore, exploiting the large number of antennas to provide integrated sensing and com-

M. Al-Jarrah and E. Alsusa are with the Department of Electrical and Electronic Engineering, University of Manchester, Manchester M13 9PL, U.K. (e-mail: {mohammad.al-jarrah, e.alsusa}@manchester.ac.uk).

C. Masouros is with the Department of Electronic and Electrical En gineering, University College London, London WC1E 7JE, U.K. (e-mail:chris.masouros@ieee.org).

This project has received funding from the European Union's Horizon 2020 research and innovation program under grant agreement No 812991.

munication (ISAC) services simultaneously is expected play a significant role in the future [7]–[13]. Therefore, this paper investigates ISAC system and studies the performance trade-off using the relative entropy (RE) theorem, or so called Kullback-Leibler divergence (KLD). Although KLD has been used in the literature to evaluate the detection capability of sensing systems [28]–[32], it is not commonly used to describe a communication systems. However, we will show that KLD can also capture the detection performance of a communication system and has a direct relation to the symbol error rate (SER). With this introduced performance measure, both subsystems, namely, the radar and the communication subsystems, can be characterized, and thus the capability of an ISAC system can be evaluated holistically using a unified performance measure rather than using a different performance measure for each individual subsystem.

A. Related Work

1) MIMO radar: In [19], MIMO based radars have been firstly proposed as an alternative solution to phased array radars, where it is shown that the new concept of MIMO radars is able to provide a spatial diversity. The performance of MIMO and phased array radars have been compared using analytical derivations for the detection and false alarm probabilities. The principle of MIMO radar is generalized to the case of non-orthogonal signal waveforms in [20]. In addition, the effect of interfering signals on the detection capability is considered in [33], and the effect of a gamma fluctuating target and synchronization errors are taken into account in [34] and [35], respectively.

The problem of target detection with MIMO radar for multi-target scenarios has also been considered in the literature [36]–[41]. In [36], for instance, the statistical angle resolution has been investigated and the performance is evaluated using derived detection and false alarm probabilities, and the clutter impact on the radar resolution is considered in [37]. A multiple hypotheses testing problem based multi-target detection is considered in [38] for passive MIMO radar in which targets illuminate signals rather that acting as scatterers or reflectors. Another effort on multi-target multi-hypothesis detection scenario using cognitive MIMO radars can be found in [39], where an adaptive waveform design algorithm is proposed. Moreover, a joint multi-target detection and localization problem is investigated in [40], where low-complex suboptimal detection algorithms have been proposed. Furthermore, a sequential probability ratio test (SPRT) based method is introduced in [41] to resolve close targets in co-located MIMO radars.

2) ISAC: More recently, ISAC systems have been introduced in the literature and attracted the attention of both academic research and industrial fields. Generally speaking, ISAC implies the use of the telecommunication network resources for both sensing and telecommunication services [10]. In such scenario, a multi-antenna BS can be applied to provide both services simultaneously by exploiting multiple beams generated in the transmission mode. In the reception mode, a portion of the antennas can be used for radar reception, or time division multiple access (TDMA) can be applied to reduce the interference. Alternatively, one can apply interference cancellation algorithms to separate radar signals from communication signals [10], [42], [43].

In [7], a robust beamforming matrix is proposed for a MU-MIMO communication system that shares the same spectrum with a MIMO radar system with the objective of maximize the detection probability of the radar system. The concept of ISAC is introduced in [8], [9] in which a single BS is dedicated for both functionalities of communications and sensing. Two models, referred to as separated deployment and shared deployment are presented, where the BS antennas are distributed among each sub-system in the separated deployment whereas all antennas are exploited for both sub-systems in the latter case. Several designs for the signals waveforms and beampatterns are proposed in [8], [9] to satisfy the requirements of communication users' rates and detection capability of the radar sub-system. A comprehensive survey for the signal processing tools that can be applied for ISAC systems can be found in [11] for three possible scenarios, namely, radar-centric, communication-centric and joint design.

In [12] and [13], a dual-functional communication and radar system with massive MIMO-OFDM is considered for downlink and uplink scenarios, respectively. The achievable rate and detection capability for both sub-systems are derived and discussed under perfect and imperfect channel side information (CSI). In [44], the dual functional system is optimized aiming at maximizing the achievable sum-rate and energy-efficiency while satisfying a minimum required target detection probability and the individual users' rates. A novel approach for ISAC system which considers IEEE 802.11ad-based long range radar operating at 60 GHz is investigated in [45], where the preamble of a single-carrier frame with good correlated sequences is exploited for the radar signal.

An optimization algorithm to jointly design the transceiver of BS and power allocation for uplink users is introduced in [46] aiming at maximizing the radar detection probability, while maintaining a desirable quality-of-service for the individual communication user equipment (CUEs). In [47], the optimal power distribution among the communication and training symbols is derived, and the waveform design is considered to maximize the weighted sum of mutual information for communication and sensing parts. Rate-splitting multiple access (RSMA) based ISAC system is introduced in [48] based on optimizing the weighted sum-rate for CUEs while satisfying a pre-defined radar beampattern under constrained average transmit power. A comprehensive literature survey about resource allocation methods is provided in [49].

Performance trade-off of ISAC system is analyzed in [50] using the detection probability and achievable rate for radar and communication users, respectively. The power resources of BS is allocated for the radar waveforms and information signals such that the probability of detection for the radar is maximized with a minimum required information rate for CUEs. In [51] and [52], the performance of uplink and downlink integrated ISAC is analyzed in terms of the outage probability, ergodic communication rate, diversity order, and sensing rate. A full-duplex ISAC scheme that exploits the waiting time of a pulsed

radar to transmit communication signals is proposed in [53]. Besides, the probability of detection for the radar sensing part and the spectrum efficiency of the communication subsystem are analyzed. In [54], an ISAC system which employs OFDM and orthogonal time frequency space (OTFS) modulation is considered, where a vehicle equipped with a mono-static radar is communicating with a receiver and simultaneously measures some parameters about that receiver by exploiting the backscattered signal. The maximum likelihood estimator and its corresponding Cramer-Rao bound have been derived for a single target scenario, and the root mean square error and data rate have been used to evaluate the performance of radar and communication subsystems, respectively. A similar setup is considered in [55] under a memoryless channel assumption and the system is analyzed using capacity-distortion trade-off, which is defined as the maximum achievable communication rate at which the data can be reliably decoded by the receiver while keeping the sensing distortion at a desirable value.

B. Motivation and Contribution

As can be depicted from the introduction and literature survey above, ISAC systems are expected to play a pivotal role in future wireless networks such as 6G and beyond. Researches in the literature usually use different metric for the performance evaluation of sensing and communication subsystems. For example, sum-rate, bit/symbol error rate, and outage probability are typically used for the communication part, whereas estimation rate, detection probability, false alarm probability and mean square error (MSE) are utilized to evaluate the performance of the radar systems. Motivated by this fact, this paper considers an ISAC system which consists of MIMO-BS serving a number of CUEs and aims at detecting a number of targets with a main objective concerns in providing a unified performance measure to evaluating the efficiency of communication and radar subsystems at the same time. The proposed performance measure is based on the Kullback-Leibler divergence theorem, also referred to the relative information theorem, which provides a measure for how different is a certain probability density function (PDF) from another one. Mathematically, it can be defined as the expectation of the log-likelihood ratio (LLR), and thus it is asymptotically related to the detection performance of radar systems. More specifically, according to Stein's lemma, a higher KLD measure implies a better detection performance for a certain radar system [30], [32].

Although KLD is well-known in the field of sensing and target detection, it is not widely used to characterize the performance of wireless communication systems. However, we will show in this paper that KLD can be employed to infer the symbol error rate of the detector at the CUEs, in addition to being informative of the detection capability of MIMO radars. Consequently, such a measure can be effectively used to evaluate the performance of ISAC systems as a single entity instead of two separated (unlinked) performance measures. Accordingly, we consider a generalized system model with a MIMO-BS, multiple users and multiple targets, where the weighted sum of the relative entropy (WSRE) is proposed to infer the efficiency of ISAC systems as one system rather than two subsystems. The contribution of this paper can be summarized in the following.

1) Providing a framework for the statistics of received signals as well as a KLD based analysis for CUEs using two well-known precoding techniques employed by the MIMO-BS, namely, the zero forcing (ZF) and the maximum ratio transmission (MRT) precoders. It is worth noting that although MRT is widely used in the literature, to the best of authors knowledge, the analysis of the statistics of the received signals and interference from other users and radar signal has not been well investigated.
2) Inspired by full-duplex communications, an interference cancellation (IC) approach, which is applicable at the MIMO-BS before employing targets detection, is proposed in order to cancel out the communication signal reflected from the environment.
3) Providing a unique KLD analysis for the MIMO radar sub-system. The uniqueness of this KLD comes from two facts. The first one is that KLD analysis with noncentral Chi-squared observations, which is the case in most of MIMO radars, has not been derived in the literature. The second fact is that the analysis takes into account the imperfect cancellation for the communication waveform portion reflected by the environment.
4) Proposing a unified performance measure for ISAC systems using WSRE for the case of multiple CUEs and targets.
5) Introducing KLD as a measure for communication systems, and illustrating its relation to SER. Additionally, the relation between KLD and the detection probability in MIMO radars is investigated.
6) Evaluating the performance of the proposed WSRE using the derived formulas, and validating the analysis by simulations.

   The obtained results show that the derived KLD is very accurate and can be efficiently used to infer the efficiency of both parts of the ISAC systems, namely, the communication and radar subsystems.

C. Paper Organization

Sec. II presents the system model for the ISAC scenario of interest and a background about KLD. Sec. III, provides the KLD analysis for the communication subsystem, and the relation between KLD and SER is investigated in Sec. IV. Sec. V shows the derivation of KLD for a MIMO radar system considering a multiple targets scenario, and relates KLD to the detection probability of radar. Sec. VI introduces the WSRE performance measure for ISAC while Sec. VII provides the numerical results and Sec. VIII concludes the paper.

II. System Model

As illustrated in Fig. 1, this work considers an ISAC system which consists of MIMO-BS with a total of N antennas serving a number of single antenna K CUEs in the downlink direction and aims at detecting T targets which can be ground targets, unmanned aerial vehicles (UAVs) or a mix of ground targets and UAVs, where the radar-targets propagation medium obeys

a line-of-sight channel model. The separated deployment, in which the BS antennas are distributed among the communication and radar subsystems, is the scenario of this paper's interest. The transmitter employs linear precoding techniques such as ZF and MRT to precode the information intended to CUEs before the transmission process takes place through the allocated $N_C \leq N$ antennas. Moreover, the power budget at BS is limited to P_{T} which is supposed to be exploited for data transmission and sensing, and thus $P_{\mathrm{T}} = P_{\mathrm{C}} + P_{\mathrm{rad}}$ where P_{C} and P_{rad} denote the amounts of power allocated for the communication and radar subsystems, respectively. It is worth mentioning that although there are several precoding methods in the literature such as interference aware precoding and dirty paper coding which could outperform ZF and MRT, the later two precoders, ZF and MRT, are the most attractive solutions due to their low-complexity, implementation feasibility in practice and reasonable performance [24]–[27]. On the other hand, the radar matrix is assumed to be designed using a desired radar signal $\mathbf{s}_l$ which satisfies a covariance matrix of $\mathbf{R}_s \triangleq \frac{1}{L}\sum_{l=1}^{L}\mathbf{s}_l\mathbf{s}_l^H$ with L being the number of snapshots. The radar signal vector $\mathbf{s}_l$ is emitted towards the targets using the remaining $N_R = N - N_C$ antennas assigned for the radar service.

A. Communication Subsystem

For a given transmission interval l, a data symbol $d_k[l]$ intended for the kth CUE is picked from a normalized constellation with $\mathbb{E}\left[|d_k[l]|^2\right] = 1$, and precoded using a linear precoder with a precoding vector $\mathbf{w}_k \in \mathbb{C}^{N_C \times 1}$, and thus the precoded information symbols for all users $\mathbf{d}_{\mathbf{w}} \in \mathbb{C}^{N_C \times 1}$ can be written as

$$\mathbf{d}_{\mathbf{w}}[l] = \sum_{i=1}^{K} \sqrt{p_i}\mathbf{w}_i d_i[l], \tag{1}$$

where p_i is a power control factor. Consequently, the received signal at the kth CUE considering the interference caused by the radar signal is

$$y_k[l] = \mathbf{g}_k^T \mathbf{d}_{\mathbf{w}}[l] + \sqrt{\frac{P_{\mathrm{rad}}}{N_R}}\mathbf{f}_k^T \mathbf{s}_l + n_k[l], \tag{2}$$

where P_{rad} is the power allocated to the radar subsystem, $\mathbf{g}_k \in \mathbb{C}^{N_C \times 1} \sim \mathcal{CN}\left(0, 2\sigma_g^2\right)$ is a flat Rayleigh channel gain vector from the communication antennas to the kth CUE, $\mathbf{f}_k^T \in \mathbb{C}^{N_R \times 1} \sim \mathcal{CN}\left(0, 2\sigma_f^2\right)$ with $(\cdot)^T$ denoting the transpose operation is a flat Rayleigh channel vector which captures the channel between the radar antennas and CUEs, $\mathbf{s}_l$ is the radar waveform, and $n_k \sim \mathcal{CN}\left(0, 2\sigma_n^2\right)$ is the additive white Gaussian noise (AWGN). In this paper, channels are assumed independent identically distributed (i.i.d) and follow flat Rayleigh fading.

B. Sensing Subsystem

Generally speaking, in MIMO radar, a signal vector $\mathbf{s}(t)$ is transmitted from BS towards the targets, which reflect the signals that are captured at the receiver, which is the same BS in the case of monostatic scenario. Moreover, due to the multipath nature of the wireless medium, the signals which get reflected from a target might be received at BS through multiple paths with different amplitudes and phases. In such scenarios, virtual targets, also known as ghost targets, which

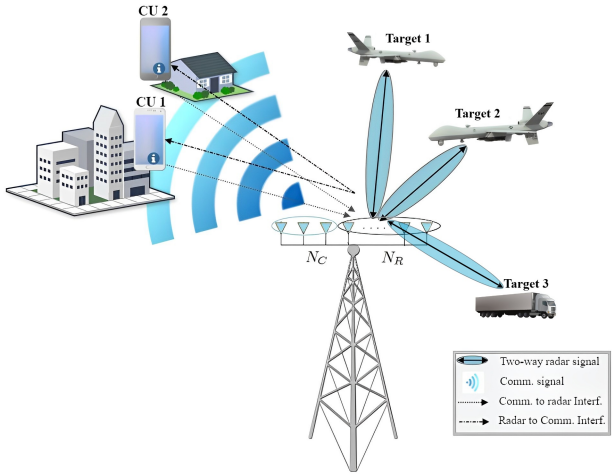

Fig. 1. An illustration diagram for separated deployment based ISAC.

are virtual copies of the actual target with different values of the angle-of-arrival (AoA), will appear. Ray tracing techniques, the uniform diffraction theory and the law of reflection can be employed to separate the actual target from ghost targets [56]–[58]. However, similar to many existing work in the literature, this work is concerned with the scenario in which the radar-targets channels are subject to direct path propagation model [20], [23], [33]. It is noteworthy mentioning that since monostatic MIMO radar with direct path channel is considered, antennas have almost equal distance to a certain target and thus they are subject to equal pathloss values. Therefore, unlike wireless communication systems, it is unlikely to have preference for one antenna over another, and thus P_{rad} can be evenly distributed over the radar antennas. Consequently, for interference free environment, the baseband representation of the radar return signals from the direct path with time delay τ_{d} and Doppler shift ω_{d} can be written as,

$$\tilde{\mathbf{y}}_{\mathrm{rad}}(t) = \sum_{t=1}^{T} \alpha_t \sqrt{\frac{P_{\mathrm{rad}}}{N_R}} \mathbf{a}_{\mathrm{R}}(\theta_t)\mathbf{a}_{\mathrm{T}}(\theta_t)^T \mathbf{s}(t - \tau_{t,\mathrm{d}}) \mathrm{e}^{j\omega_{t,\mathrm{d}}t} + \mathbf{n}_{\mathrm{rad}}(t), \tag{3}$$

where α_t is the channel gain for BS-Target-BS path, $\mathbf{a}_{\mathrm{T}}(\theta_t)$ and $\mathbf{a}_{\mathrm{R}}(\theta_t)$ denote the transmit and receive array gain, respectively, and $\mathbf{n}_{\mathrm{rad}}(t)$ is AWGN. The received signals vector $\tilde{\mathbf{y}}_{\mathrm{rad}}(t)$ is typically processed through a bank of matched filters which are tuned to a Doppler frequency of ω_{d} and a time delay of τ_{d}. In other words, the detection process is applied to a certain range-Doppler bin and could be repeated for other range-Doppler bins separately [20], [23], [33]. Therefore, let the desired radar waveform in signal domain $\mathbf{s}_l \in \mathbb{C}^{N_R \times 1}\ \forall l \leq L$, where L is the number of snapshots, $\mathbf{a}_{\mathrm{T}}(\theta)$ and $\mathbf{a}_{\mathrm{R}}(\theta)$ are the transmit and receive array gains of a uniform linear array (ULA), respectively, the signals vector reflected by the targets and received at BS, which is processed through a bank of filters tuned to τ_{d} and ω_{d} and impinged by communication signal interference, can be expressed as

$$\tilde{\mathbf{y}}_{\mathrm{rad}}[l] = \sum_{t=1}^{T} \alpha_t \sqrt{\frac{P_{\mathrm{rad}}}{N_R}} \mathbf{a}_{\mathrm{R}}(\theta_t)\mathbf{a}_{\mathrm{T}}(\theta_t)^T \mathbf{s}_l + \mathbf{G}_{\mathrm{rad}}\mathbf{d}_{\mathbf{w}}[l] + \mathbf{n}_{\mathrm{rad}}[l], \tag{4}$$

where the term $\mathbf{G}_{\rm rad}\mathbf{d}_{\mathbf{w}}[l]$ represents the interference from the communication subsystem which is caused by backscattering the communication signal from the environment, $\mathbf{G}_{\rm rad} \in \mathbb{C}^{N_R \times N_C}$ is the channel matrix from the N_C communication antennas to N_R radar antennas, and $\mathbf{n}_{\rm rad} \in \mathbb{C}^{N_R \times 1}$is the AWGN, i.e., $\mathbf{n}_{\rm rad} \sim \mathcal{CN}\left(0, 2\sigma_n^2 \mathbf{I}_{N_R}\right)$ where $\mathbf{I}_{N_R}$ is the identity matrix. It should be observed that typical radar systems are designed such that $\mathbf{s}_l$ satisfies a desired covariance matrix $\mathbf{R}_{\mathbf{s}} = \frac{1}{L}\sum_{l=1}^{L} \mathbf{s}_l \mathbf{s}_l^H$, for example, $\mathbf{R}_{\mathbf{s}} = \mathbf{I}_{N_C}$ for omnidirectional radars.

Interestingly, it can be observed from (4) that the interference caused by the communication signal consists of the channel gain of the BS (Communication transmitter)-Environment-BS (radar receiver) link and the data vector $\mathbf{d}_{\mathbf{w}}[l]$ which has been already transmitted from BS. Since $\mathbf{d}_{\mathbf{w}}[l]$ is previously known at BS, interference cancellation (IC) process can be very beneficial if the estimate of $\mathbf{G}_{\rm rad}$ is available at BS. It worth noting that the estimation of $\mathbf{G}_{\rm rad}$ can be performed at BS in a previous phase through pilot signals. Therefore, inspired by full duplex communication systems, we propose such IC process which is very useful for real life ISAC systems and analyze the radar system considering that the IC process is not perfect. Given the estimated channel matrix $\hat{\mathbf{G}}_{\rm rad}$, the received signals in (4) after applying IC can be rewritten as

$$\mathbf{y}_{\rm rad}[l] = \sum_{t=1}^{T} \alpha_t \sqrt{\frac{P_{\rm rad}}{N_R}} \mathbf{A}(\theta_t)\mathbf{s}_l + \omega_{\rm rad}[l] + \mathbf{n}_{\rm rad}[l], \quad (5)$$

where a monostatic radar is considered with $\mathbf{a}(\theta_t) \triangleq \mathbf{a}_{\rm R}(\theta_t) = \mathbf{a}_{\rm T}(\theta_t) \triangleq \left[1, \mathrm{e}^{j\frac{2\pi\Delta}{\lambda_0}\sin\theta_t}, \cdots, \mathrm{e}^{j\frac{2\pi\Delta}{\lambda_0}(N_R-1)\sin\theta_t}\right]^T$, Δ is the antenna spacing, λ_0 is the signal wavelength, $\mathbf{A}(\theta_t) \in \mathbb{C}^{N_R \times N_R} = \mathbf{a}(\theta_t)\mathbf{a}(\theta_t)^T$ is the equivalent array manifold, and $\omega_{\rm rad}[l] \in \mathbb{C}^{N_R \times 1} = \mathbf{G}_{\rm err}\mathbf{d}_{\mathbf{w}}[l] = \mathbf{G}_{\rm err}\sum_{k=1}^{K}\sqrt{p_k}\mathbf{w}_k d_k[l]$ is the interference from the communication subsystem to radar subsystem after employing IC with $\mathbf{G}_{\rm err} \triangleq \mathbf{G}_{\rm rad} - \hat{\mathbf{G}}_{\rm rad}$ representing channel estimation errors.

C. The Relative Entropy or Kullback-Leibler Divergence (KLD)

The relative entropy, or KLD, for a pair of random PDFs is defined in **Definition 1** below. Although the KLD measure is originally defined for a pair of PDFs, it can be extended for multiple PDFs by considering every pair separately and then evaluating the average for all possible unequal pairs.

Definition 1: For a pair of continuous probability density functions (PDFs), $f_m(x)$ and $f_n(x)$, $\mathrm{KLD}_{n\to m}$ is defined as the relative entropy from $f_n(x)$ to $f_m(x)$ or a measure of how different a PDF $f_n(x)$ is from another PDF $f_m(x)$. In general , KLD is an asymmetric measure, and mathematically $\mathrm{KLD}_{n\to m}$ for continuous random variable can be represented as [30]

$$\mathrm{KLD}(f_m \parallel f_n) = \int_{-\infty}^{\infty} f_m(x)\log_2\left(\frac{f_m(x)}{f_n(x)}\right)dx, \quad (6)$$

where $\mathrm{KLD}(f_m \parallel f_n) \triangleq \mathrm{KLD}_{n\to m} \forall m \neq n$. For multivariate Gaussian distributed random variables having mean vectors of μ_m and μ_n and covariance matrices of Σ_m and Σ_n, it can be derived as

$$\mathrm{KLD}_{n\to m} = \frac{1}{2\ln 2}\Big(\mathrm{tr}\left(\Sigma_n^{-1}\Sigma_m\right) - 2 + (\mu_{k,n} - \mu_{k,m})^T \times \Sigma_n^{-1}(\mu_{k,n} - \mu_{k,m}) + \ln\frac{|\Sigma_n|}{|\Sigma_m|}\Big), \quad (7)$$

Since KLD is generally asymmetric, the average KLD can be evaluated wherever $\mathrm{KLD}_{n\to m} \neq \mathrm{KLD}_{m\to n}$, i.e., $\mathrm{KLD}_{n,m} \triangleq \frac{1}{2}(\mathrm{KLD}_{n\to m} + \mathrm{KLD}_{m\to n})$. It worth noting that when the logarithm function with base 2, i.e., $\log_2(\cdot)$, is considered, KLD is measured in bits, whereas it is measured in nats when the natural logarithm $\ln(\cdot)$ is used. In this work, we consider the first case and KLD is measured in bits.

KLD, or the relative entropy, has a wide range of applications in several science and engineering disciplines such as comparing the information gain of different statistical models for model selection, machine learning to measure the information gain achieved by using the distribution f_m rather than the current distribution f_n, information coding to measure the expected number of extra bits required to encode samples taken from the distribution f_m using a code optimized for another distribution f_n, and quantum information science where the minimum $\mathrm{KLD}(f_m \parallel f_n)$ over all possible separable states f_n is used to model the entanglement in state f_m. According to the well known Neyman-Pearson lemma, the best way to separate or distinguish between two random variables through an observation X taken from one of them is obtained by using the log-likelihood ratio test, i.e., $\log_2(\frac{f_m(x)}{f_n(x)})$, where the performance can be assessed using the expected value of the log-likelihood ratio which represents the relative entropy or KLD as defined in (6). Moreover, $\mathrm{KLD}_{n\to m}$, or equivalently $\mathrm{KLD}(f_m \parallel f_n)$, with f_m and f_n respectively represent the distribution of received samples under hypotheses H_1 and H_0, can be interpreted as the expected discrimination information or information gain for discriminating hypothesis H_1 against hypothesis H_0 when H_1 is the true hypothesis [59]–[62].

Clearly, KLD is an informative measure that can be applied for inferring systems to assess the discrimination process between a set of candidates such as the data detection process in communication systems and hypothesis testing problem in sensing systems. Moreover, unlike traditional metrics such as SER, detection probability and false alarm probability, KLD is independent of the detection process and detection thresholds applied at the receiver. By using KLD as a unified performance measure, the performance of the two subsystems of ISAC are put on the same scale rather than two different scales. It is noteworthy to mention that according to [30, Ch. 2], KLD is a generalization for the concept of mutual information which in one role generalizes the Shannon entropy. Therefore, our core aim in this work is to develop a unified performance framework for both sensing and communications, departing from separate performance metrics, which is very beneficial for the design of integrated waveforms for ISAC systems. Additionally, it is worth noting that the trade-off between the two subsystems is not always clear when different metrics are employed to evaluate the performance of ISAC.

III. Relative Entropy Analysis for Communication Subsystem

The received signal at the kth CUE in (2) can be represented as

$$y_k[l] = \sqrt{p_k}\mathbf{g}_k^T\mathbf{w}_k d_k[l] + \mathbf{g}_k^T\sum_{\substack{i=1\\ i\neq k}}^{K}\sqrt{p_i}\mathbf{w}_i d_i[l] + \eta_k[l], \quad (8)$$

where $\eta_k[l] \triangleq \sqrt{\frac{P_{\rm rad}}{N_R}}\mathbf{f}_k^T\mathbf{s}_l + n_k[l]$ is the radar interference plus noise. It can be shown that the distribution of $\mathbf{f}_k^T\mathbf{s}_l$ follows complex Gaussian with a mean of $\mathbb{E}\left[\mathbf{f}_k^T\mathbf{s}_l\right]=0$ and a variance of

$$\mathbb{E}\left[\mathbf{f}_k^H\mathbf{s}_l\mathbf{s}_l^H\mathbf{f}_k\right] = 2\sigma_f^2\mathbb{E}\left[\mathrm{tr}\left(\mathbf{s}_l\mathbf{s}_l^H\right)\right] = 2\sigma_f^2\mathrm{tr}(\mathbf{R}_s) = 2\sigma_f^2 N_R, \quad (9)$$

where the last equality is obtained given the fact that the elements of the main diagonal of $\mathbf{R}_s$ are typically normalized to ones. Consequently, the distribution of $\eta_k[l] = \sqrt{\frac{P_{\rm rad}}{N_R}}\mathbf{f}_k^T\mathbf{s}_l + n_k[l]$ is complex Gaussian with $\eta_k[l] \sim \mathcal{CN}\left(0, 2\sigma_\eta^2\right)$ where $\sigma_\eta^2 = P_{\rm rad}\sigma_f^2 + \sigma_n^2$.

For the design of the data beamforming matrix $\mathbf{W} = [\mathbf{w}_1, \mathbf{w}_2, \cdots, \mathbf{w}_K]$, we consider the widely accepted ZF and MRT in the following two sections. Generally speaking, for a linear precoding matrix $\mathbf{W}$, the received data vector at CUEs can be written in a matrix form as

$$\mathbf{y}[l] = \mathbf{G}^T\mathbf{W}\mathbf{P}\mathbf{d}[l] + \eta, \quad (10)$$

where $\mathbf{G} \in \mathbb{C}^{N_C\times K} = [\mathbf{g}_1, \mathbf{g}_2, \cdots, \mathbf{g}_K]$, $\mathbf{W} \in \mathbb{C}^{N_C\times K} = [\mathbf{w}_1, \mathbf{w}_2, \cdots, \mathbf{w}_K]$ is the precoding matrix, $\mathbf{P} \in \mathbb{C}^{K\times K} = \mathrm{diag}\left(\sqrt{p_1}, \sqrt{p_2}, \cdots, \sqrt{p_K}\right)$ is power control matrix, $\mathbf{d} \in \mathbb{C}^{K\times 1} = [d_1[l], d_2[l], \cdots, d_K[l]]^T$, $\mathbf{F} \in \mathbb{C}^{N_R\times K} = \left[\mathbf{f}_1^T, \mathbf{f}_2^T, \cdots, \mathbf{f}_K^T\right]$ is the interfering channel matrix between the radar antennas and CUEs, $\mathbf{n} \in \mathbb{C}^{K\times 1} = [n_1[l], n_2[l], \cdots, n_K[l]]^T$, and $\eta \in \mathbb{C}^{K\times 1} = [\eta_1[l], \eta_2[l], \cdots, \eta_K[l]]^T$, which is defined as $\eta \triangleq \sqrt{\frac{P_{\rm rad}}{N_R}}\mathbf{F}^T\mathbf{s}_l + \mathbf{n}$, is the radar interference plus noise term with $\eta_k \sim \mathcal{CN}\left(0, 2\sigma_\eta^2\right)$ where $\sigma_\eta^2 = P_{\rm rad}\sigma_f^2 + \sigma_n^2$.

A. ZF based Data Precoding

Here, we assume ZF is employed at BS to precode the users' data, which is able to cancel out the interference between the users. Using such precoder, the precoding matrix $\mathbf{W}$ is generally given by $\mathbf{W} = \mathbf{G}^*\left(\mathbf{G}^T\mathbf{G}^*\right)^{-1}$, where $(\cdot)^*$ is the conjugate operator. Consequently, by substituting $\mathbf{W}$ in (10) and noting that $\mathbf{G}^T\mathbf{W} = \mathbf{I}_K$ with $\mathbf{I}_K$ represents the identity matrix, we obtain

$$\mathbf{y}[l] = \mathbf{P}\mathbf{d}[l] + \eta, \quad (11)$$

where $\mathbf{P}$ depends on the normalization scheme employed as discussed in the next two subsections.

1) ZF based on vector normalization: With vector normalization based ZF (VNZF), $\mathbf{P} = \mathrm{diag}\left(\alpha_{1,\rm ZF}, \alpha_{2,\rm ZF}, \cdots, \alpha_{K,\rm ZF}\right)\mathbf{P}_{\rm com}$ where $\alpha_{k,\rm ZF} = \frac{1}{\|\mathbf{w}_k\|}$ is a normalization factor and $\mathbf{P}_{\rm com} \triangleq \mathrm{diag}\left(\sqrt{P_{1,\rm com}}, \sqrt{P_{2,\rm com}}, \cdots, \sqrt{P_{K,\rm com}}\right)$ with constraint $P_{\rm C} = \sum_k P_{k,\rm com}$ is used to control the average transmission power for CUEs. It is worthy to mention that for users with equal priorities, $P_{k,\rm com}$ can be selected such that $P_{k,\rm com} = \frac{P_{\rm C}}{K}$. Anyway, for the general case with unequal $P_{k,\rm com}$'s, the received signal at the kth CUE is

$$y_k[l] = \sqrt{P_{k,\rm com}}\alpha_{k,\rm ZF}d_k[l] + \eta_k[l]. \quad (12)$$

Based on the received signal $y_k[l]$, the conditional density function of $y_k|\{d_k[l], \alpha_{k,\rm ZF}\}$ is complex Gaussian (or bivariate Gaussian), which can be expressed as

$$f\left(y_k|\{d_k[l], \alpha_{k,\rm ZF}\}\right) = \frac{\exp\left(-\left(\mathbf{y}_k-\mu_k\right)^T\Sigma^{-1}\left(\mathbf{y}_k-\mu_k\right)\right)}{\sqrt{\left(2\pi\right)^2|\Sigma|}}, \quad (13)$$

where $\mathbf{y}_k \triangleq [y_{k,\Re}, y_{k,\Im}]^T$ with $y_{k,\Re} \triangleq \mathrm{Re}\left(y_k\right)$ and $y_{k,\Im} = \mathrm{Im}\left(y_k\right)$ denote the real and imaginary components of y_k, respectively, and $\mu_k \triangleq [\mu_{k,\Re}, \mu_{k,\Im}]^T$ with $\mu_{k,\Re} = \sqrt{P_{k,\rm com}}\alpha_{k,\rm ZF}\mathrm{Re}\left(d_k[l]\right)$ and $\mu_{k,\Im} = \sqrt{P_{k,\rm com}}\alpha_{k,\rm ZF}\mathrm{Im}\left(d_k[l]\right)$. The covariance matrix $\Sigma = \sigma_\eta^2\mathbf{I}_2$ with $|\Sigma| = \sigma_\eta^4$ and $\Sigma^{-1} = \frac{1}{\sigma_\eta^2}\mathbf{I}_2$.

Corollary 1: For a generalized M-ary signal constellation, KLD can be evaluated for each possible pair of unequal data symbols $\{d_{k,n}[l], d_{k,m}[l]\}, n \neq m$. Let us consider a pair of symbols $\left\{d_{k,n}[l] \triangleq |a_{k,n}|\,e^{j\phi_{k,n}}, d_{k,m}[l] \triangleq |a_{k,m}|\,e^{j\phi_{k,m}}\right\}\forall n \neq m$, with corresponding received signals density functions $f_n \sim \mathcal{CN}\left(\mu_{k,n}, \Sigma_n\right)$ and $f_m \sim \mathcal{CN}\left(\mu_{k,m}, \Sigma_m\right)$, thus the relative entropy for the kth CUE measured in bits from f_m to f_n is denoted as $\mathrm{KLD}_{m\to n}$ and can be derived using **Definition 1** as

$$\mathrm{KLD}_{k,m\to n} = \frac{1}{2\ln 2}\Big(\mathrm{tr}\left(\Sigma_m^{-1}\Sigma_n\right) - 2 + \left(\mu_{k,m}-\mu_{k,n}\right)^H \times\Sigma_m^{-1}\left(\mu_{k,m}-\mu_{k,n}\right) + \ln\frac{|\Sigma_m|}{|\Sigma_n|}\Big). \quad (14)$$

By noting that $\Sigma_n = \Sigma_m = \sigma_\eta^2\mathbf{I}_2$, and given that $\mu_{k,m} = \left[\sqrt{P_{k,\rm com}}\alpha_{k,\rm ZF}\cos\phi_{k,m}, \sqrt{P_{k,\rm com}}\alpha_{k,\rm ZF}\sin\phi_{k,m}\right]$, $\mathrm{KLD}_{m\to n}$ can be simplified to

$$\begin{aligned}\mathrm{KLD}_{k,m\to n} &= \frac{1}{2\sigma_\eta^2\ln 2}\left(\mu_{k,m}-\mu_{k,n}\right)^H\left(\mu_{k,m}-\mu_{k,n}\right)\\ &= \frac{\gamma_{\rm VNZF}}{\ln 2}\Big(|a_m|^2+|a_n|^2-2|a_m||a_n|\cos(\phi_{k,m}-\phi_{k,n})\Big)\\ &= \frac{\gamma_{\rm VNZF}}{\ln 2}\left|d_{k,n}[l]-d_{k,m}[l]\right|^2, \end{aligned} \quad (15)$$

where $\gamma_{k,\rm VNZF} = \frac{\alpha_{k,\rm ZF}^2 P_{k,\rm com}}{2\sigma_\eta^2}$.

As stated earlier, since KLD is measured for a pair of PDFs, the average KLD, $\mathrm{KLD}_{k,\rm VNZF}$, is evaluated by considering all possible pairs of dissimilar symbols, which can be represented as

$$\mathrm{KLD}_{k,\rm VNZF} = \frac{\gamma_{\rm VNZF}}{\ln 2}\sum_{m=1}^{M}\sum_{\substack{n=1\\ n\neq m}}^{M}\Pr(\phi_{k,m},\phi_{k,n})\left|d_{k,n}[l]-d_{k,m}[l]\right|^2, \quad (16)$$

and for equal likelihood symbols, it can be reduced to

$$\begin{aligned}\mathrm{KLD}_{k,\rm VNZF} &= \frac{\gamma_{\rm VNZF}}{M(M-1)\ln 2}\sum_{m=1}^{M}\sum_{\substack{n=1\\ n\neq m}}^{M}\left|d_{k,n}[l]-d_{k,m}[l]\right|^2\\ &= \frac{\lambda}{M\left(M-1\right)\ln 2}\gamma_{\rm VNZF}, \end{aligned} \quad (17)$$

where $\lambda = \sum_{m=1}^{M}\sum_{\substack{n=1\\n\neq m}}^{M}\left|d_{k,n}\left[l\right]-d_{k,m}\left[l\right]\right|^2$ which depends on the transmitted data constellation, and thus λ is a constant for a given constellation. For MPSK signalling, as an example, with a normalized constellation, $\mathrm{KLD}^{\mathrm{MPSK}}_{k,\mathrm{VNZF},m\to n} = \frac{2}{\ln 2}\gamma_{\mathrm{VNZF}} \times\left(1-\cos\left(\phi_{k,m}-\phi_{k,n}\right)\right)$ and $\mathrm{KLD}^{\mathrm{MPSK}}_{k,\mathrm{VNZF}} = \frac{\lambda}{M\left(M-1\right)\ln 2}\gamma_{\mathrm{VNZF}}$ with $\lambda_{\mathrm{MPSK}} = 2\sum_{m=1}^{M}\sum_{\substack{n=1\\n\neq m}}^{M}\left(1-\cos\left(\phi_{k,m}-\phi_{k,n}\right)\right)$ are obtained.

The KLD derivations have not considered the randomness nature of the communication channel so far, which results in a random normalization factor $\alpha_{k,\mathrm{ZF}}$, and thus averaging over $\alpha_{k,\mathrm{ZF}}$ must be taken into account for the sake of completeness. Towards this goal, the distribution of $\alpha^2_{k,\mathrm{ZF}} \triangleq \frac{1}{\left[\left(\mathbf{G}^T\mathbf{G}^*\right)^{-1}\right]_{k,k}}$ is found first, which under Rayleigh fading follows a Gamma random variable with a scale factor of 1 and a shape factor of $L_{\mathrm{G}} = N_C - K + 1$ [63], i.e., $x \triangleq \alpha^2_{k,\mathrm{ZF}} \sim \mathrm{Gamma}(L_{\mathrm{G}},1)$.

$$f_x\left(x\right) = \frac{1}{\Gamma\left(L_{\mathrm{G}}\right)}x^{L_{\mathrm{G}}-1}\mathrm{e}^{-x}, x\geq 0. \tag{18}$$

Therefore, $\alpha_{k,\mathrm{ZF}}$ follows the generalized Gamma distribution with the following PDF

$$f_{\alpha_{k,\mathrm{ZF}}}\left(\alpha_{k,\mathrm{ZF}}\right) = \frac{2}{\Gamma\left(L_{\mathrm{G}}\right)}\alpha^{2L_{\mathrm{G}}-1}_{k,\mathrm{ZF}}\mathrm{e}^{-\alpha^2_{k,\mathrm{ZF}}}, \alpha_{k,\mathrm{ZF}}\geq 0. \tag{19}$$

Consequently, by evaluating the average of (17) the relative entropy for the kth CUE is

$$\mathrm{KLD}_{k,\mathrm{IVNZF,avg}} = \frac{\lambda}{M\left(M-1\right)\ln 2}\mathbb{E}\left[\gamma_{\mathrm{VNZF}}\right]. \tag{20}$$

Substituting the density function given by (19) in (20), $\mathrm{KLD}_{k,\mathrm{IVNZF,avg}}$ can be expressed as

$$\mathrm{KLD}_{k,\mathrm{IVNZF,avg}} = \frac{\lambda}{M\left(M-1\right)\ln 2}\frac{P_{k,\mathrm{com}}}{2\sigma^2_\eta}\frac{2}{\Gamma\left(L_{\mathrm{G}}\right)} \times\int_0^\infty \alpha^{2L_{\mathrm{G}}+1}_{k,\mathrm{ZF}}\mathrm{e}^{-\alpha^2_{k,\mathrm{ZF}}}d\alpha_{k,\mathrm{ZF}}. \tag{21}$$

By using integration by substitution with $y=\alpha^2_{k,\mathrm{ZF}}$, and noting that $\alpha^{2L_{\mathrm{G}}}_{k,\mathrm{ZF}} = \left(\alpha^2_{k,\mathrm{ZF}}\right)^{L_{\mathrm{G}}} = y^{L_{\mathrm{G}}}$ and $d\alpha_{k,\mathrm{ZF}} = \frac{1}{2\alpha_{k,\mathrm{ZF}}}dy$, $\mathrm{KLD}_{k,\mathrm{IVNZF,avg}}$ is reduced to

$$\mathrm{KLD}_{k,\mathrm{IVNZF,avg}} = \frac{\lambda}{M\left(M-1\right)\ln 2}\frac{P_{k,\mathrm{com}}}{2\sigma^2_\eta}\frac{1}{\Gamma\left(L_{\mathrm{G}}\right)} \times\int_0^\infty y^{L_{\mathrm{G}}}\mathrm{e}^{-y}dy. \tag{22}$$

Thereafter, with the aid of the definition of the Gamma function, i.e., $\Gamma\left(L_{\mathrm{G}}\right) = \int_0^\infty y^{L_{\mathrm{G}}-1}\mathrm{e}^{-y}dy$, thus $\int_0^\infty y^{L_{\mathrm{G}}}\mathrm{e}^{-y}dy = \Gamma\left(L_{\mathrm{G}}+1\right)$, and using the fact that $\Gamma\left(L_{\mathrm{G}}+1\right) = L_{\mathrm{G}}!$ since L_{G} is a positive integer value, $\mathrm{KLD}_{k,\mathrm{IVNZF,avg}}$ can be found as

$$\mathrm{KLD}_{k,\mathrm{IVNZF,avg}} = \frac{\lambda}{M\left(M-1\right)\ln 2}\frac{P_{k,\mathrm{com}}}{2\sigma^2_\eta}L_{\mathrm{G}}. \tag{23}$$

2) ZF with instantaneous matrix normalization: With instantaneous channel matrix based normalization, $\mathbf{P} \triangleq \tilde{\alpha}_{\mathrm{ZF}}\mathbf{P}_{\mathrm{com}}$ with $\tilde{\alpha}_{\mathrm{ZF}} = \sqrt{\frac{1}{\left(\mathbf{d}^H\mathbf{W}\mathbf{W}^H\mathbf{d}\right)}}$, and the received signal at the kth CUE can be written as

$$y_k\left[l\right] = \sqrt{P_{k,\mathrm{com}}}\tilde{\alpha}_{\mathrm{ZF}}d_k\left[l\right]+\eta_k[l]. \tag{24}$$

Following the derivations in the previous case, it can be easily shown that $\tilde{\alpha}_{\mathrm{ZF}}$ follows a generalized Gamma distribution, i.e., $\tilde{\alpha}_{\mathrm{ZF}} \sim \mathrm{GG}(a=1, d=2L_{\mathrm{G}} = 2\left(N_C-K+1\right), p=2)$. Based on the received signal $y_k\left[l\right]$, the density function of $y_k|\left\{\tilde{\alpha}_{\mathrm{ZF}}, d_k\left[l\right]\right\}$ is complex Gaussian (or bivariate Gaussian), and thus the instantaneous and average KLD for the kth CUE can be respectively expressed as

$$\mathrm{KLD}_{k,\mathrm{IZF}|\alpha_{\mathrm{ZF}}} = \frac{\lambda}{M\left(M-1\right)\ln 2}\frac{P_{k,\mathrm{com}}}{2\sigma^2_\eta}\tilde{\alpha}^2_{\mathrm{ZF}}, \tag{25}$$

with an average value of

$$\mathrm{KLD}_{k,\mathrm{IZF,avg}} = \frac{\lambda}{M(M-1)\ln 2}\frac{P_{k,\mathrm{com}}}{2\sigma^2_\eta}\int_0^\infty \tilde{\alpha}^2_{\mathrm{ZF}}f_{\tilde{\alpha}_{\mathrm{ZF}}}(\tilde{\alpha}_{\mathrm{ZF}})d\tilde{\alpha}_{\mathrm{ZF}}. \tag{26}$$

By substituting the generalized Gamma distribution for $f_{\tilde{\alpha}_{\mathrm{ZF}}}\left(\tilde{\alpha}_{\mathrm{ZF}}\right)$, and then employing the integration by substitution theorem with $x=\tilde{\alpha}^2_{\mathrm{ZF}}$ and using the definition of Gamma function, $\mathrm{KLD}_{k,\mathrm{IZF,avg}}$ can be derived as

$$\mathrm{KLD}_{k,\mathrm{IZF,avg}} = \frac{\lambda}{M\left(M-1\right)\ln 2}\frac{P_{k,\mathrm{com}}}{2\sigma^2_\eta}\left(N_C-K+1\right). \tag{27}$$

Interestingly, by comparing (27) with (23), it can be realized that the KLDs for ZF with instantaneous vector normalization and matrix normalization are equal. Therefore, we will consider ZF with instantaneous matrix normalization in our investigations henceforth.

B. MRT based Data Precoding with Vector Normalization

To employ MRT, sometimes called the matched filter (MF), for data precoding, the precoding vector for the kth user data, $\mathbf{w}_k$, is evaluated based on the channel vector $\mathbf{g}_k$ only, and thus $\mathbf{w}_k$ is independent of $\mathbf{g}_i \forall i\neq k$. For MRT, we consider the instantaneous vector based normalization with $\mathbf{w}_k = \mathbf{g}^*_k$ and thus the received signal at the kth user can be written as

$$\begin{aligned} y_k\left[l\right] &= \mathbf{g}^T_k\sum_{i=1}^{K}\sqrt{P_{i,\mathrm{com}}}\frac{\mathbf{w}_i}{\left\|\mathbf{g}_i\right\|}d_i\left[l\right]+\sqrt{\frac{P_{\mathrm{rad}}}{N_R}}\mathbf{f}^T_k\mathbf{s}_l+n_k[l] \\ &= \sqrt{P_{k,\mathrm{com}}}\left\|\mathbf{g}_k\right\|d_k\left[l\right]+\tilde{\omega}_{\mathrm{MRT}}, \end{aligned} \tag{28}$$

where the equivalent inter-user and radar interference plus noise term $\tilde{\omega}_{\mathrm{MRT}} = \omega_{\mathrm{MRT}}+\eta_k[l]$ with $\omega_{\mathrm{MRT}} = \mathbf{g}^T_k\sum_{\substack{i=1\\i\neq k}}^{K}\sqrt{P_{i,\mathrm{com}}}\breve{\mathbf{g}}_i d_i\left[l\right]$ is the inter-user interference, where $\breve{\mathbf{g}}_i = \mathbf{g}^*_i/\left\|\mathbf{g}_i\right\|$. To find the statistical distribution of $\tilde{\omega}_{\mathrm{MRT}}$, we first evaluate the statistical properties of ω_{MRT}. Towards this goal, let us define new variables as $\tilde{v}_{k,i} = \sqrt{P_{i,\mathrm{com}}}\frac{t_{k,i}}{z_i}$, $z_i = \left\|\mathbf{g}_i\right\| \triangleq \sqrt{\sum_{n_c=1}^{N_C}\left|\mathbf{g}_{i,n_c}\right|^2}$, and $t_{k,i} = \sum_{n_c=1}^{N_C}d_i\left[l\right]\mathbf{g}^T_{k,n_c}\mathbf{g}^*_{i,n_c}\forall i\neq k$, and thus ω_{MRT} can be written as

$$\omega_{\mathrm{MRT}} = \sum_{\substack{i=1\\i\neq k}}^{K}\sqrt{P_{i,\mathrm{com}}}\frac{\sum_{n_c=1}^{N_C}d_i\left[l\right]\mathbf{g}^T_{k,n_c}\mathbf{g}^*_{i,n_c}}{\left\|\mathbf{g}_i\right\|} = \sum_{\substack{i=1\\i\neq k}}^{K}\tilde{v}_{k,i}. \tag{29}$$

As shown in Appendix I, with the aid of the central limit theorem (CLT), the density of $\tilde{v}_{k,i}$ can be approximated as a complex Gaussian distribution, $\tilde{v}_{k,i} \sim \mathcal{CN}\left(0, 2P_{i,\mathrm{com}}\sigma^2_v\right)$, and thus $\omega_{\mathrm{MRT}} \sim \mathcal{CN}\left(0, 2\sigma^2_v\sum_{\substack{i=1\\i\neq k}}^{K}P_{i,\mathrm{com}}\right)$. Therefore, the equivalent inter-user and radar interference plus noise $\tilde{\omega}_{\mathrm{MRT}} \sim \mathcal{CN}\left(0, 2\sigma^2_\omega\right)$ where $\sigma^2_\omega = \sigma^2_v\sum_{\substack{i=1\\i\neq k}}^{K}P_{i,\mathrm{com}}+\sigma^2_\eta$ with

$\sigma_\eta^2 = P_{\rm rad}\sigma_f^2 + \sigma_n^2$. Fig. 2 compares the density functions obtained by approximation (Aprx) with the actual distributions obtained by simulation (Sim) for different values of the number of communication antennas N_C, where the total number of the BS antennas is fixed at $N = 30$. Binary phase shift keying (BPSK) is considered in this figure with $\frac{P_{\rm T}}{\sigma_n^2} = 10$ dB, $P_{\rm rad} = 0.3$ units and the number of CUEs is $K = 2$. It is worth noting that the legends for Fig. 2 a) and Fig. 2 b) are similar, as well as, the legend of Fig. 2 d) is the same as Fig. 2 c). Since the variables $t_{k,i}$, $\tilde{v}_{k,i}$ and $\tilde{\omega}_{\rm MRT}$ are complex and symmetric, we plot the real components of the random variables as the imaginary parts have distributions identical to the real parts. As can noted from the figure, the accuracy of CLT considered to approximate the PDF of $t_{k,i}$ starts improving as N_C increases. More specifically, the approximated PDF converges to simulations for $N_C > 8$. It can be also observed from Fig. 2 b) that the Gaussian approximation used in Appendix I to approximate the Chi squared distributed random variable z_i is very accurate for $N_C > 4$. As can be seen from Fig. 2 b), unlike the other three subfigures, the mean value of z_i increases as N_C increases which can be attributed to the fact that z_i is the envelope of the sum of the power gains of a number of N_C independent paths according to the definition of z_i above (29). On the other hand, it can be observed from Fig. 2 a) that the mean value of $t_{k,i}$ is 0 since it is a sum of i.i.d random variables with zero mean, and so are $\tilde{v}_{k,i}$ and $\tilde{\omega}_{\rm MRT}$ as seen from Fig. 2 c) and Fig. 2 d). Interestingly, as can be depicted from Fig. 2 c) and Fig. 2 d), the variance of $\tilde{v}_{k,i}$ and $\tilde{\omega}_{\rm MRT}$ is independent of N_C because, according to their definition, each term is normalized by $\|\mathbf{g}_i\|$ which cancels the impact of N_C. Interestingly, Fig. 2 c) and Fig 2 d) show that the distributions of $\tilde{v}_{k,i}$ and $\tilde{\omega}_{\rm MRT}$ are independent of the number of antennas N_C and the approximated densities perfectly captures the characteristics of these random variables.

Since the distribution of $\tilde{\omega}_{\rm MRT}$ is accurately approximated as a Gaussian density function, **Corollary 1** can be employed and then the expected value with respect to $\|\mathbf{g}_k\|^2$ is evaluated. Consequently, the KLD for MRT with vector based normalization can be found as

$$\begin{aligned}\mathrm{KLD}_{k,\mathrm{NIMRT,avg}} &= \frac{P_{k,\rm com}}{2\sigma_\omega^2 M\left(M-1\right)\ln 2}\lambda\mathbb{E}\left[\|\mathbf{g}_k\|^2\right] \\ &= \frac{\lambda\sigma_g^2}{\sigma_\omega^2 M\left(M-1\right)\ln 2}N_C P_{k,\rm com}, \quad (30)\end{aligned}$$

where the fact that $\|\mathbf{g}_k\|^2 \sim \mathrm{Gamma}\left(N_C, 2\sigma_g^2\right)$ is used to evaluate $\mathbb{E}\left[\|\mathbf{g}_k\|^2\right]$.

IV. Relation Between ZF-KLD and SER

For the sake of completeness, in this section we compare the commonly used SER performance evaluation metric with the KLD metric. Towards this purpose, we consider the ZF precoding scheme with instantaneous matrix based power normalization whose received signal is given in (24). The SER of most standard modulation schemes, such as MPSK, MPAM, rectangular and nonrectangular MQAM, under AWGN channel can be generally approximated as [64, Table 6.1, pp. 180],

$$\mathrm{SER}_{\mathrm{IZF}|\tilde{\alpha}_{\rm ZF}} = AQ\left(\sqrt{B\gamma_{\mathrm{IZF}|\tilde{\alpha}_{\rm ZF}}}\right), \quad (31)$$

where $\gamma_{\mathrm{IZF}|\tilde{\alpha}_{\rm ZF}} \triangleq \frac{P_{k,\rm com}}{2\sigma_\eta^2}\tilde{\alpha}_{\rm ZF}^2$ and $\mathrm{SER}_{\mathrm{IZF}|\tilde{\alpha}_{\rm ZF}}$ denote the instantaneous SNR and SER, respectively, of an IMZF based precoding system conditioned on $\tilde{\alpha}_{\rm ZF}$, $Q\left(\cdot\right)$ is the tail distribution function of the standard normal distribution, i.e., the Q-function, and the values of A and B are constants which are dependent on the modulation scheme and order. Consequently, by comparing (25) with (31), the KLD in (25) can be written in terms of $\mathrm{SER}_{\mathrm{LTZF}|\tilde{\alpha}_{\rm ZF}}$ as

$$\mathrm{KLD}_{\mathrm{IZF}|\tilde{\alpha}_{\rm ZF}} = \frac{\lambda}{M(M-1)\ln 2}\frac{1}{B}\left(Q^{-1}\left(\frac{\mathrm{SER}_{\mathrm{IZF}|\tilde{\alpha}_{\rm ZF}}}{A}\right)\right)^2, \quad (32)$$

where $Q^{-1}\left(\cdot\right)$ is the inverse Q-function. On the other hand, the average SER can be evaluated by averaging $\mathrm{SER}_{\mathrm{IZF}|\tilde{\alpha}_{\rm ZF}}$ over the PDF of $\tilde{\alpha}_{\rm ZF}$, which can be written as

$$\mathrm{SER}_{\rm IZF} = A\int_0^\infty Q\left(\sqrt{\frac{BP_{k,\rm com}}{2\sigma_\eta^2}}\tilde{\alpha}_{\rm ZF}\right) f_{\tilde{\alpha}_{\rm ZF}}(\tilde{\alpha}_{\rm ZF})d\tilde{\alpha}_{\rm ZF}. \quad (33)$$

By substituting the PDF of $\tilde{\alpha}_{\rm ZF}$ provided in (19) and rewriting the Q-function in terms of the complementary error function erfc, i.e., $Q\left(x\right) = \frac{1}{2}\mathrm{erfc}\left(\frac{1}{\sqrt{2}}x\right)$, $\mathrm{SER}_{\rm IZF}$ can be expressed as

$$\begin{aligned}\mathrm{SER}_{\rm IZF} = \frac{A}{\Gamma\left(N_C-K+1\right)}\int_0^\infty \tilde{\alpha}_{\rm ZF}^{2(N_C-K)+1}\mathrm{e}^{-\tilde{\alpha}_{\rm ZF}^2} \\ \times \mathrm{erfc}\left(\sqrt{\frac{BP_{k,\rm com}}{4\sigma_\eta^2}}\tilde{\alpha}_{\rm ZF}\right)d\tilde{\alpha}_{\rm ZF}, \quad (34)\end{aligned}$$

which can be solved using [65, 2.8.5.6, pp. 104] as

$$\begin{aligned}\mathrm{SER}_{\rm IZF} = A\left(\frac{1}{2} - \frac{\Gamma\left(N_C-K+1.5\right)}{\Gamma\left(N_C-K+1\right)}\sqrt{\frac{BP_{k,\rm com}}{4\pi\sigma_\eta^2}}\right. \\ \left.\times\ {}_2F_1\left(\left[0.5, N_C-K+1.5\right]; 1.5; -\frac{BP_{k,\rm com}}{4\sigma_\eta^2}\right)\right), \quad (35)\end{aligned}$$

where ${}_2F_1\left(\left[\ \cdot\ ,\ \cdot\ \right];\cdot\ ;\cdot\right)$ is the Gaussian, or ordinary, hypergeometric function. By comparing $\mathrm{SER}_{\mathrm{IZF}|\tilde{\alpha}_{\rm ZF}}$ with the average KLD in (27), it is more convenient to rewrite $\mathrm{SER}_{\mathrm{IZF}|\tilde{\alpha}_{\rm ZF}}$ as a function of KLD. Therefore, by using (27), we obtain $\frac{P_{k,\rm com}}{2\sigma_\eta^2} = \frac{M\left(M-1\right)\ln 2}{\lambda\left(N_C-K+1\right)}\mathrm{KLD}_{\rm IZF,avg}$, and thus $\mathrm{SER}_{\rm IZF}$ can be rewritten as

$$\begin{aligned}\mathrm{SER}_{\rm IZF} = A\left(\frac{1}{2} - \frac{\Gamma\left(N_C-K+1.5\right)}{\Gamma\left(N_C-K+1\right)}\sqrt{\frac{B\tilde{\lambda}}{2\pi}\mathrm{KLD}_{\rm IZF,avg}}\right. \\ \left.\times\ {}_2F_1\left(\left[0.5, N_C-K+1.5\right]; 1.5; -\frac{B}{2}\tilde{\lambda}\mathrm{KLD}_{\rm IZF,avg}\right)\right), \quad (36)\end{aligned}$$

where $\tilde{\lambda} = \frac{M\left(M-1\right)\ln 2}{\left(N_C-K+1\right)\lambda}$.

V. Radar System with Multiple Targets

For the radar subsystem, we consider the case in which targets are spatially separated such that each target is in a distinct radar bin [41], [66], [67]. It is worth noting that some separation algorithms have been proposed in the literature to separate signals associated with individual targets in the case

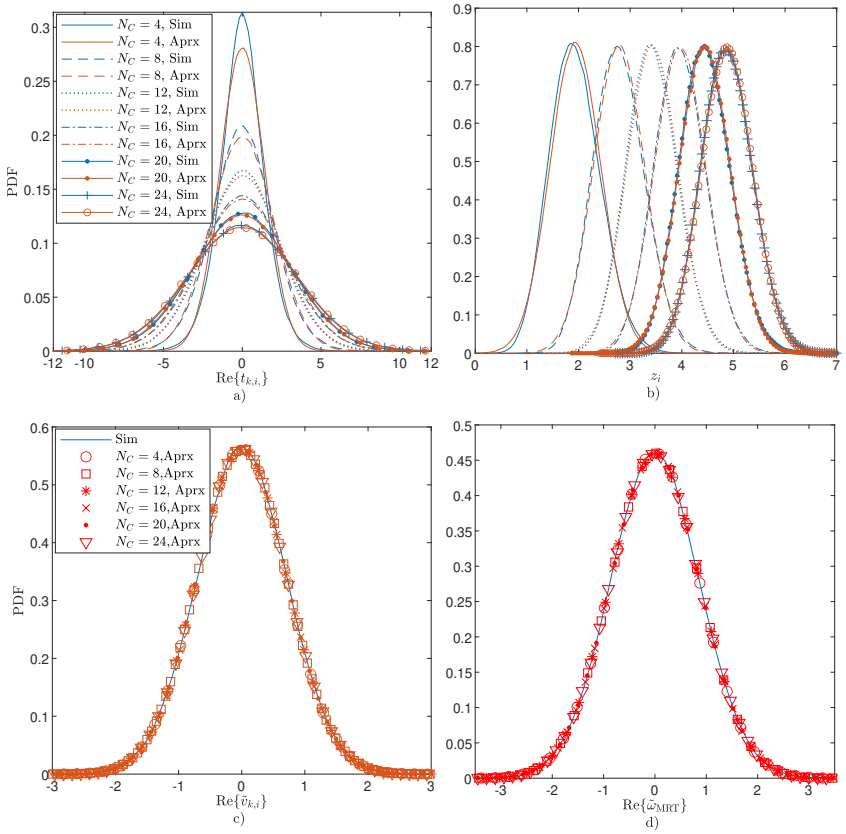

Fig. 2. The density functions of the approximated random variables: a) The PDF of the real part of $t_{i,k}$, b) The PDF of z_i, c) The PDF of the real part of $\tilde{v}_{i,k}$, and d) The PDF of the real part of interference plus SNR $\tilde{\omega}_{\mathrm{MRT}}$.

of unresolvable targets, and thus estimating the number of targets can be achieved accordingly, [38]–[40]. We assume that the number of possibly existing targets in the environment is known at BS, however, a simple counting method can be performed by employing the detection process in this paper on all radar angular-range-Doppler bins and then counting the number of detected targets. Additionally, we consider that MIMO radar is able to generate multiple beams simultaneously by considering a linear combination of multiple orthogonal signals [21], [68]–[70]. Let $\Phi = [\phi_1, \phi_2, \cdots, \phi_T]^T$ be a set of T orthonormal baseband waveforms, κ_t with $\sum_{t=1}^{T} \kappa_t = 1$ is a power allocation factor which is used to control the amount of power to be emitted towards a certain target, and $\mathbf{w}_{\mathrm{rad},t}[l] \in \mathbb{C}^{N_R \times 1}, t = \{1, 2, \cdots, T\}$ is a weight vector at the lth signalling period, then the transmitted signals vector at the output of transmitting antennas can be represented as

$$\tilde{\mathbf{s}}_l = \sqrt{\frac{P_{t,\mathrm{rad}}}{N_R}} \sum_{t=1}^{T} \sqrt{\kappa_t} \mathbf{w}_{\mathrm{rad},t}[l] \phi_t = \sqrt{\frac{P_{t,\mathrm{rad}}}{N_R}} \mathbf{W}_{\mathrm{rad}} \mathrm{diag}(\bar{\kappa}) \Phi, \tag{37}$$

where $\bar{\kappa} \in \mathbb{C}^{1 \times T} = \left[\sqrt{\kappa_1}, \sqrt{\kappa_2}, \cdots, \sqrt{\kappa_T}\right]$ with $\|\bar{\kappa}\|^2 = 1$ is the power allocation vector that is used to control the portion of power emitted towards each target, and $\mathbf{W}_{\mathrm{rad}}[l] \in \mathbb{C}^{N_R \times T} = [\mathbf{w}_{\mathrm{rad},1}[l], \mathbf{w}_{\mathrm{rad},2}[l], \cdots, \check{\mathbf{w}}_{\mathrm{rad},T}[l]]$ with $\mathbf{w}_{\mathrm{rad},t}[l] \in \mathbb{C}^{N_R \times 1}$ is the precoding matrix. In general, the precoding vectors $\mathbf{w}_{\mathrm{rad},t}[l] \forall t$ can be designed to optimize the radar subsystem performance or satisfy some desired radar covariance matrix; for example, a radar covariance matrix of $\mathbf{R}_{\mathbf{w}} \triangleq \frac{1}{L} \mathbf{W}_{\mathrm{rad}} \times \mathbf{W}_{\mathrm{rad}}^H = \mathbf{I}_{N_R \times N_R}$ is typically used for omnidirectional radar. Using this signal waveform design for the radar subsystem, the receiver can apply a set of matched filters to separate the signals reflected by different targets by matched-filtering the received signals $\mathbf{y}_{\mathrm{rad}}(t)$ to signal waveforms $\phi_t \forall t = \{1, 2, \cdots, T\}$. Consequently, after matched-filtering $\mathbf{y}_{\mathrm{rad}}$ under hypothesis H_1, the target existence scenario, using the corresponding ϕ_t, the received signal vector in baseband in (5) can be rewritten as

$$\mathbf{y}_{\mathrm{rad},t|H_1}[l] = \sqrt{\frac{\kappa_t P_{\mathrm{rad}}}{N_R}} \alpha_t \mathbf{a}_{\mathrm{R}}(\theta_t) \mathbf{a}_{\mathrm{T}}(\theta_t)^T \mathbf{w}_{\mathrm{rad},t}[l] + \mathbf{G}_{\mathrm{rad}} \mathbf{d}_{\mathbf{w}}[l] + \mathbf{n}_{\mathrm{rad}}[l], \tag{38}$$

where the last equality is obtained using the fact that $\phi_t \forall t = \{1, 2, \cdots, T\}$ are orthonormal waveforms. Interestingly, as can be observed from the received signal form, the interference and noise free part of $\mathbf{y}_{\mathrm{rad},t}[l] \in \mathbb{C}^{N_R \times 1}$ is a function of the parameters of target t only, and thus targets can be resolved and detected independently of each other.

By employing IC to cancel out or reduce the amount of interference caused by the communication signals reflected by the environment and noting that we consider imperfect cancellation due to channel estimation errors of $\mathbf{G}_{\mathrm{err}}$, then the received signal vector under hypothesis H_1 can be represented as

$$\check{\mathbf{y}}_{\mathrm{rad},t|H_1}[l] = \sqrt{\frac{\kappa_t P_{\mathrm{rad}}}{N_R}} \alpha_t \mathbf{A}(\theta) \mathbf{w}_{\mathrm{rad},t}[l] + \omega_{\mathrm{rad}} + \mathbf{n}_{\mathrm{rad}}[l], \tag{39}$$

where $\omega_{\rm rad} \in \mathbb{C}^{N_R\times 1} \triangleq \mathbf{G}_{\rm err}\mathbf{d}_{\mathbf{w}}\left[l\right] = \mathbf{G}_{\rm err}\sum_{i=1}^{K}\sqrt{p_i}\mathbf{w}_i d_i\left[l\right]$ represents the residue of the communication signal after implementing IC. By assuming that the statistics of channel estimation errors follow a Gaussian distribution [71], [72], i.e., each entry of $\mathbf{G}_{\rm err}$ is $\mathcal{CN}\left(0, 2\sigma_{\rm err}^2\right)$ where $2\sigma_{\rm err}^2$ is the variance of the channel estimator, and noting that every element in $\omega_{\rm rad}$ is a sum of independent KN_C random variables, the CLT can be applied to approximate the density of the elements of $\omega_{\rm rad}$ for large KN_C. Consequently, the errors caused by imperfect IC are approximately complex Gaussian distributed, $\omega_{\rm rad} \sim \mathcal{CN}\left(0, 2\sigma_{\omega}^2\mathbf{I}_{N_R}\right)$ with $\sigma_{\omega}^2 = \sigma_{\rm err}^2\sigma_{\rm w}^2 N_C \times\sum_{i=1}^{K} P_{i,\rm com}$ where $\sigma_{\rm w}^2$ is the variance of the elements of $\mathbf{w}_i$. Hence, the received signal can be expressed as

$$\check{\mathbf{y}}_{{\rm rad},t|H_1}\left[l\right] = \sqrt{\frac{\kappa_i P_{\rm rad}}{N_R}}\alpha_t\mathbf{A}\left(\theta_t\right)\mathbf{w}_{{\rm rad},t}[l] + \tilde{\omega}_{\rm rad}, \quad (40)$$

where $\tilde{\omega}_{\rm rad} \triangleq \omega_{\rm rad} + \mathbf{n}_{\rm rad}\left[l\right] \sim \mathcal{CN}\left(0, 2\sigma_{\tilde{\omega}}^2\mathbf{I}_{N_R}\right)$ with $\sigma_{\tilde{\omega}}^2 = \sigma_{\omega}^2 + \sigma_n^2$.

On the other hand, under null hypothesis H_0, i.e., the target absence scenario, the received signals consist of the residues of imperfect IC and AWGN, consequently, the received signals vector is

$$\check{\mathbf{y}}_{{\rm rad}|H_0}\left[l\right] = \tilde{\omega}_{\rm rad}. \quad (41)$$

After collecting a number of L snapshots, the received signal matrix can be formulated as

$$\check{\mathbf{Y}}_{{\rm rad},t|H_1} = \sqrt{\frac{\kappa_i P_{\rm rad}}{N_R}}\alpha_t\mathbf{a}_{\rm R}\left(\theta_t\right)\mathbf{a}_{\rm T}^{T}\left(\theta_t\right)\mathbf{W}_{{\rm rad},t} + \mathbf{\Omega}_{\rm rad} \quad (42)$$

$$\check{\mathbf{Y}}_{{\rm rad},t|H_0} = \mathbf{\Omega}_{\rm rad}, \quad (43)$$

where $\tilde{\mathbf{W}}_{t,\rm rad} \in \mathbb{C}^{N_R\times L} = [\mathbf{w}_{t,\rm rad}[1], \mathbf{w}_{t,\rm rad}[2], \cdots, \mathbf{w}_{t,\rm rad}[L]]$ and $\mathbf{\Omega}_{\rm rad}\in\mathbb{C}^{N_R\times L} = [\tilde{\omega}_{t,\rm rad}[1], \tilde{\omega}_{t,\rm rad}[2], \cdots, \tilde{\omega}_{t,\rm rad}[L]]$. By noting that $\check{\mathbf{y}}_{{\rm rad},t|H_1}[l]\sim\mathcal{CN}\left(\sqrt{\frac{\kappa_i P_{\rm rad}}{N_R}}\alpha_t\mathbf{A}(\theta_t)\mathbf{w}_{{\rm rad},t}[l], 2\sigma_{\tilde{\omega}}^2\mathbf{I}_{N_R}\right)$, the log-likelihood function of the received signal matrix $\check{\mathbf{Y}}_{{\rm rad},t|H_1}$ can be obtained as

$$\ln\left(f\left(\check{\mathbf{Y}}_{{\rm rad},t|H_1};\alpha_t,\theta_t\right)\right) = -N_R L\ln\left(\pi\sigma_{\tilde{\omega}}^2\right) - \frac{1}{2\sigma_{\tilde{\omega}}^2} \times\sum_{l=1}^{L}\left\|\check{\mathbf{y}}_{{\rm rad},t|H_1}\left[l\right] - \sqrt{\frac{\kappa_i P_{\rm rad}}{N_R}}\alpha_t\mathbf{A}\left(\theta_t\right)\mathbf{w}_{{\rm rad},t}\left[l\right]\right\|^2. \quad (44)$$

By evaluating the squared norm and neglecting the terms which do not affect the estimation process, the sufficient statistic matrix can be formulated as

$$\tilde{\mathbf{E}}_t = \frac{1}{L}\sum_{l=1}^{L}\check{\mathbf{y}}_{{\rm rad},t|H_1}\left[l\right]\mathbf{w}_{{\rm rad},t}^{H}\left[l\right], \quad (45)$$

which, after extracting the independent sufficient statistics, can be simplified to [20, Eq. 15],

$$\mathbf{e}_t = \alpha_t\mathbf{d}_{\mathbf{w}}\left(\theta_t\right) + \tilde{\mathbf{n}}, \quad (46)$$

where $\mathbf{d}_{\mathbf{w}}\left(\theta_t\right) = {\rm vec}\left\{\mathbf{A}\left(\theta_t\right)\mathbf{U}\mathbf{\Lambda}^{1/2}\right\}$ with $\breve{\mathbf{w}}_{{\rm rad},t}\left[l\right] = \mathbf{\Lambda}^{-1/2}\mathbf{U}^{H}\mathbf{w}_{{\rm rad},t}\left[l\right]$ denotes the equivalent array steering vector which is a function of the signal correlation matrix, and $\tilde{\mathbf{n}} = \frac{1}{L}{\rm vec}\left\{\sum_{l=1}^{L}\tilde{\omega}_{\rm rad}\left[l\right]\breve{\mathbf{w}}_{{\rm rad},t}^{H}\left[l\right]\right\} \sim \mathcal{CN}\left(0, 2\sigma_{\tilde{\omega}}^2\mathbf{I}_{N_R}\right)$. Consequently, the generalized likelihood ratio test (GLRT) can be formulated as $\xi\left(\theta_t\right) \underset{H_0}{\overset{H_1}{\lessgtr}} \tau$, where τ is a detection threshold which, according to Neyman-Pearson test, is determined by fixing the false alarm rate at a fixed value, and $\xi\left(\theta_t\right)$ is the generalized likelihood ratio function and given by [73, Ch. 6.5]

$$\xi(\theta_t) \triangleq \ln\left(\frac{\arg\max_{\theta_t,\alpha_t} f(\mathbf{e}_t;\alpha_t,\theta_t,H_1)}{\arg\max_{\theta_t,\alpha_t} f(\mathbf{e}_t;H_0)}\right) = \ln\left(\frac{f\left(\mathbf{e}_t;\hat{\alpha}_t,\hat{\theta}_t,H_1\right)}{f\left(\mathbf{e}_t;H_0\right)}\right), \quad (47)$$

where $\left\{\hat{\alpha}_t, \hat{\theta}_t\right\}$ are the maximum likelihood estimates of the target parameters, which can be evaluated as

$$\left\{\hat{\alpha}_t,\hat{\theta}_t\right\} = \arg\max_{\theta_t,\alpha_t} f(\mathbf{e}_t;\alpha_t,\theta_t,H_1) = \arg\min_{\theta_t,\alpha_t}\left\|\mathbf{e}_t - \alpha_t\mathbf{d}_{\mathbf{w}}(\theta_t)\right\|^2. \quad (48)$$

The generalized likelihood ratio function $\xi\left(\theta_t\right)$ can be derived as [20, Eq. 36]

$$\xi(\theta_t) = \left|\mathbf{a}_{\rm R}^{H}\left(\hat{\theta}_t\right)\tilde{\mathbf{E}}_t\mathbf{a}_{\rm T}\left(\hat{\theta}_t\right)\right|^2 / \left(N_R\mathbf{a}_{\rm R}^{H}\left(\hat{\theta}_t\right)\mathbf{R}_t^{T}\mathbf{a}_{\rm T}\left(\hat{\theta}_t\right)\right), \quad (49)$$

where $\mathbf{R}_t = \frac{1}{L}\sum_{l=1}^{L}\mathbf{w}_{t,\rm rad}\left[l\right]\mathbf{w}_{t,\rm rad}^{H}\left[l\right]$. After substituting for $\tilde{\mathbf{E}}_t$ as given in (45), $\xi\left(\theta_t\right)$ can be written as

$$\xi\left(\theta_t\right) = \frac{\left|\mathbf{a}_{\rm R}^{H}\left(\hat{\theta}_t\right)\frac{1}{L}\sum_{l=1}^{L}\check{\mathbf{y}}_{{\rm rad},t|H_1}\left[l\right]\mathbf{w}_{{\rm rad},t}^{H}\left[l\right]\mathbf{a}_{\rm T}\left(\hat{\theta}_t\right)\right|^2}{N_R\mathbf{a}_{\rm R}^{H}\left(\hat{\theta}_t\right)\mathbf{R}_t^{T}\mathbf{a}_{\rm T}\left(\hat{\theta}_t\right)}. \quad (50)$$

Thereafter, by using the law of large numbers, it can be deduced that at $L \longrightarrow \infty$, the estimators of α_t and θ_t are asymptotically consistent estimators, thus $\hat{\theta}_t \overset{asymp.}{\longrightarrow} \theta_t$ and $\hat{\alpha}_t \overset{asymp.}{\longrightarrow} \alpha_t$. Consequently, by substituting for $\check{\mathbf{y}}_{{\rm rad},t|H_1}$ using (40) and considering orthogonal signal waveforms with $\mathbf{R}_t = \mathbf{I}_{N_R}$, $\xi\left(\theta_t\right)$ can be reduced to

$$\xi\left(\theta_t\right) = \left|\left(\sqrt{\frac{\kappa_i P_{\rm rad}}{N_R}}\alpha_t\mathbf{a}_{\rm T}\left(\theta_t\right)^{T}\mathbf{R}_t\mathbf{a}_{\rm T}\left(\hat{\theta}_t\right) + \breve{n}\right)\right|^2, \quad (51)$$

where $\breve{n} \sim \mathcal{CN}\left(0, 2\sigma_{\tilde{\omega}}^2\right)$. Obviously, by using the fact that the squared amplitude of a complex Gaussian distributed random variable is Chi-squared distributed, the sufficient statistics of $\xi\left(\theta_k\right)$ is [20, Eq. 37], [33, Eq. 54], [73, Ch. 6.5]

$$\xi\left(\theta_t\right) \sim \begin{cases} H_1 : \mathcal{X}_2^2\left(\lambda_t\right) \\ H_0 : \mathcal{X}_2^2\left(0\right) \end{cases}, \quad (52)$$

where $\mathcal{X}_2^2\left(\lambda_t\right)$ denotes a noncentral Chi-squared random variable with 2 degrees of freedom and a noncentrality parameter of $\lambda_t = |\alpha_t|^2\kappa_t P_{\rm rad}\left|\mathbf{a}^{H}\left(\theta_t\right)\mathbf{R}_t\mathbf{a}\left(\theta_t\right)\right|^2/(\sigma_{\tilde{\omega}}^2 N_R)$, which for orthogonal waveforms (e.g. $\mathbf{R}_t = \mathbf{I}_{N_R}$ where $\mathbf{I}_{N_R}$ is an $N_R\times N_R$ identity matrix), can be reduced to $\lambda_t = |\alpha_t|^2\kappa_t N_R P_{\rm rad}/\sigma_{\tilde{\omega}}^2$.

A. KLD from ξ_{H_1} to ξ_{H_0}

By using **Definition 1**, noting that noncentral Chi-squared random variables are strictly positive, substituting $f_{\xi}\left(\xi|H_0\right) = \frac{1}{2}{\rm e}^{-0.5\xi}$ and $f_{\xi}\left(\xi|H_1\right) = \frac{1}{2}{\rm e}^{-0.5(\xi+\lambda_t)}I_0\left(\sqrt{\lambda_t\xi}\right)$, and using the logarithmic identity $\log_2 x = \ln x/\ln 2$, the relative information from ξ_{H_1} to ξ_{H_0} can be derived as

$$\begin{aligned}{\rm KLD}\left(\xi_{H_0}\parallel\xi_{H_1}\right) &= \int_0^{\infty} f_{\xi}\left(\xi|H_0\right)\log_2\left(\frac{f_{\xi}\left(\xi|H_0\right)}{f_{\xi}\left(\xi|H_1\right)}\right)d\xi \\ &= \frac{1}{2\ln 2}\int_0^{\infty}{\rm e}^{-0.5\xi}\ln\left(\frac{1}{{\rm e}^{-0.5\lambda_t}I_0\left(\sqrt{\lambda_t\xi}\right)}\right)d\xi. \end{aligned} \quad (53)$$

Thereafter, using the logarithmic identities $\log_a\left(x/y\right) = \log_a x - \log_a y$ and $\log_a\left(xy\right) = \log_a x + \log_a y$, and noting that

$\ln(1)=0$, $\ln(\mathrm{e}^{x})=x$ and $\int_{0}^{\infty}\mathrm{e}^{-0.5\xi}=2$, $\mathrm{KLD}\left(\xi_{H_0}\parallel\xi_{H_1}\right)$ can be written as (54) on page 12.

To be able to solve the integral, we make use of the infinite series representation of the modified Bessel function $I_0(x)$ for $0\leq x\leq 1$, and an asymptotic approximation for $I_0(x)$ which is very accurate for $x>1$. It is worth noting that since $I_0(x)$ is sharply increasing as x increases, thus the computation of the infinite series representation is very costly for large values of x. Therefore, the infinite series representation of $I_0(x)$ is employed for small values of x, i.e., $0\leq x\leq 1$, while an efficient asymptotic approximation with high accuracy is invoked when $x>1$ [74, Eq. 9.7.1, pp. 377]. Using the infinite series representation, $I_0\left(\sqrt{\lambda_t\xi}\right)$for $0\leq\xi\leq 1/\lambda_t$(e.g. the Bessel function argument $x\in[0,1]$) can be written as [74, Eq. 9.6.10, pp. 375],

$$I_0\left(\sqrt{\lambda_t\xi}\right)=1+\sum_{l=1}^{\infty}\frac{\lambda_t^l}{2^{2l}\left(l!\right)^2}\xi^l, 0\leq\xi\leq\frac{1}{\lambda_t}. \tag{55}$$

However, since this representation will be used for small values of $\lambda_t\xi$, the first few terms, i.e., two or three terms, provide a tractable solution with a very accurate approximation. On the other hand, the following approximation is used for $\xi>1/\lambda_t$ [74, Eq. 9.7.1, pp. 377],

$$I_0\left(\sqrt{\lambda_t\xi}\right)\simeq\frac{\exp\left(\sqrt{\lambda_t\xi}\right)}{\sqrt{2\pi}\sqrt[4]{\lambda_t\xi}}\left(1+\sum_{q=1}^{Q}\left(\frac{1}{\left(\sqrt{\lambda_t\xi}\right)^q}\times\frac{\prod_{k=1}^{q}\left[\left(2k-1\right)^2\right]}{q!8^q}\right)\right),\xi>\frac{1}{\lambda_t}, \tag{56}$$

where the results show that using $Q=5$ provide very accurate approximation for the considered scenarios in this paper. Consequently, by dividing the interval of the integral in (54) into two subintervals as discussed above, $\mathrm{KLD}\left(\xi_{H_0}\parallel\xi_{H_1}\right)$ can be given by

$$\mathrm{KLD}\left(\xi_{H_0}\parallel\xi_{H_1}\right)=\frac{1}{2}\left(1.4427\lambda_t-\frac{1}{\ln 2}\left(\mathcal{I}_1+\mathcal{I}_2\right)\right), \tag{57}$$

where

$$\mathcal{I}_1=\int_{0}^{\frac{1}{\lambda_t}}\mathrm{e}^{-0.5\xi}\ln\left(I_0\left(\sqrt{\lambda_t\xi}\right)\right)d\xi, \tag{58}$$

and

$$\mathcal{I}_2=\int_{\frac{1}{\lambda_t}}^{\infty}\mathrm{e}^{-0.5\xi}\ln\left(I_0\left(\sqrt{\lambda_t\xi}\right)\right)d\xi. \tag{59}$$

By substituting the infinite series representation (55) in (58), $\mathcal{I}_1$ can be written as

$$\mathcal{I}_1=\int_{0}^{\frac{1}{\lambda_t}}\mathrm{e}^{-0.5\xi}\ln\left(1+\sum_{l=1}^{\infty}\frac{\lambda_t^l}{2^{2l}\left(l!\right)^2}\xi^l\right)d\xi. \tag{60}$$

Thereafter, the Taylor series expansion for $\ln(1+x)$ is invoked [75, Eq. 1.511, pp. 53]. However, by noting that for the considered range of ξ, i.e., $\xi<\frac{1}{\lambda_t}$, $\sum_{l=1}^{\infty}\frac{\lambda_t^l}{2^{2l}(l!)^2}\xi^l<1$, using the first term of Taylor series expansion can be considered, i.e., $\ln(1+x)\approx x$ for $x<1$. Consequently, using the fact that summation and integration are interchangeable, $\mathcal{I}_1$ can be rewritten as

$$\mathcal{I}_1=\sum_{l=1}^{\infty}\frac{\lambda_t^l}{2^{2l}\left(l!\right)^2}\int_{0}^{\frac{1}{\lambda_t}}\mathrm{e}^{-0.5\xi}\xi^l d\xi, \tag{61}$$

which, after evaluating the integral and some mathematical manipulations, can be evaluated as

$$\mathcal{I}_1=\sum_{l=1}^{\infty}\frac{\lambda_t^{0.5l}\mathrm{e}^{-\frac{0.25}{\lambda_t}}}{2^{1.5l-1}\left(l+1\right)\left(l!\right)^2}\mathrm{M}_{0.5l,0.5l+0.5}\left(\frac{0.5}{\lambda_t}\right), \tag{62}$$

where $\mathrm{M}_{\cdot,\cdot}(\cdot)$ is the Whittaker-M function.

On the other hand, substituting the approximation given by (56) in (59) yields

$$\mathcal{I}_2\approx\sqrt{\lambda_t}\mathcal{I}_{2a}-\left(\left(\frac{1}{2}\ln\left(2\pi\right)+\frac{1}{4}\ln\left(\lambda_t\right)\right)\mathcal{I}_{2b}+\frac{1}{4}\mathcal{I}_{2c}\right)+\mathcal{I}_{2d}, \tag{63}$$

where the derivations of $\mathcal{I}_{2a}$, $\mathcal{I}_{2b}$, $\mathcal{I}_{2c}$ and $\mathcal{I}_{2a}$ are provided in Appendix II.

B. KLD from ξ_{H_0} to ξ_{H_1}

Similar to the previous subsection, the KLD from ξ_{H_0} to ξ_{H_1}, i.e., $\mathrm{KLD}\left(\xi_{H_1}\parallel\xi_{H_0}\right)$, can be derived with the aid of **Definition 1** as

$$\mathrm{KLD}\left(\xi_{H_1}\parallel\xi_{H_0}\right)=\int_{-\infty}^{\infty}f_{\xi}\left(\xi|H_1\right)\log_2\left(\frac{f_{\xi}\left(\xi|H_1\right)}{f_{\xi}\left(\xi|H_0\right)}\right)d\xi. \tag{64}$$

By employing the logarithmic identity $\log(x/y)=\log x-\log y$, substituting the PDFs of $f_{\xi}\left(\xi|H_0\right)$ and $f_{\xi}\left(\xi|H_1\right)$, and using some simple mathematical operations, $\mathrm{KLD}\left(\xi_{H_1}\parallel\xi_{H_0}\right)$ can be found as

$$\begin{aligned}\mathrm{KLD}\left(\xi_{H_1}\parallel\xi_{H_0}\right)&=\frac{-0.5\lambda_t\mathrm{e}^{-0.5\lambda_t}}{2\ln 2}\mathcal{I}_3+\frac{\mathrm{e}^{-0.5\lambda_t}}{2\ln 2}\mathcal{I}_4\\&=\frac{-0.5\lambda_t}{\ln 2}+\frac{\mathrm{e}^{-0.5\lambda_t}}{2\ln 2}\mathcal{I}_4,\end{aligned} \tag{65}$$

where $\mathcal{I}_3=\int_{0}^{\infty}\mathrm{e}^{-0.5\xi}I_0\left(\sqrt{\lambda_t\xi}\right)d\xi$ which has been solved using [65, Eq. 2.15.5.4, pp. 306], and $\mathcal{I}_4$ is given by

$$\mathcal{I}_4=\int_{0}^{\infty}\mathrm{e}^{-0.5\xi}I_0\left(\sqrt{\lambda_t\xi}\right)\ln\left(I_0\left(\sqrt{\lambda_t\xi}\right)\right)d\xi. \tag{66}$$

Similar to the procedure applied to evaluate $\mathrm{KLD}\left(\xi_{H_0}\parallel\xi_{H_1}\right)$, the infinite series representation for the modified Bessel function and the asymptotic approximation for $0\leq\xi\leq 1/\lambda_t$ and $\xi>1/\lambda_t$, respectively. Thus the integral $\mathcal{I}_4$ can be tightly approximated as

$$\begin{aligned}\mathcal{I}_4=&\underbrace{\int_{0}^{\frac{1}{\lambda_t}}\mathrm{e}^{-0.5\xi}I_0\left(\sqrt{\lambda_t\xi}\right)\ln\left(I_0\left(\sqrt{\lambda_t\xi}\right)\right)d\xi}_{\mathcal{I}_{4a}}\\&+\underbrace{\int_{\frac{1}{\lambda_t}}^{\infty}\mathrm{e}^{-0.5\xi}I_0\left(\sqrt{\lambda_t\xi}\right)\ln\left(I_0\left(\sqrt{\lambda_t\xi}\right)\right)d\xi}_{\mathcal{I}_{4b}}.\end{aligned} \tag{67}$$

The evaluation of $\mathcal{I}_{4a}$ and $\mathcal{I}_{4a}$ is provided with details in Appendix III.

C. The Detection and False Alarm Probabilities

For the sake of completeness, this subsection compares the commonly used detection probability metric with the KLD

$$\mathrm{KLD}(\xi_{H_0}\|\,\xi_{H_1})=\frac{1}{2}\left(\frac{0.5\lambda_t}{\ln 2}\int_{-\infty}^{\infty}\mathrm{e}^{-0.5\xi}d\xi-\frac{1}{\ln 2}\int_{-\infty}^{\infty}\mathrm{e}^{-0.5\xi}\ln\left(I_0\left(\sqrt{\lambda_t\xi}\right)\right)d\xi\right)=\frac{1}{2}\left(1.4427\lambda_t-\frac{1}{\ln 2}\int_{0}^{\infty}\mathrm{e}^{-0.5\xi}\ln\left(I_0\left(\sqrt{\lambda_t\xi}\right)\right)\right)d\xi. \quad (54)$$

measure. The detection and false alarm probabilities are respectively defined as

$$P_{\mathrm{D}}\triangleq\int_{\tau}^{\infty}f_{\xi}\left(\xi|H_1\right)d\xi=1-F_{\xi}\left(\tau|H_1\right)=Q_1\left(\sqrt{\lambda_t},\sqrt{\tau}\right), \quad (68)$$

and

$$P_{\mathrm{FA}}\triangleq\int_{\tau}^{\infty}f_{\xi}\left(\xi|H_0\right)d\xi=1-F_{\xi}\left(\tau|H_0\right)=Q_1\left(0,\sqrt{\tau}\right)=\Gamma(1,0.5\tau), \quad (69)$$

where $F_{\xi}\left(\xi|H_i\right)\forall i=\{0,1\}$ is the cumulative distribution function (CDF) of ξ under hypothesis H_i, $\Gamma\left(\cdot,\cdot\right)$ is the upper incomplete gamma function, $Q_1\left(\sqrt{\lambda_t},\sqrt{\tau}\right)$ is the Marcum Q-function, and τ is a predefined threshold which according to Neyman-Pearson lemma is selected to satisfy a certain false alarm constraint, for example, $\tau=2\Gamma^{-1}\left(1,P_{\mathrm{FA}}\right)$ with $\Gamma^{-1}\left(1,\cdot\right)$ is the inverse incomplete Gamma function. Consequently, the detection probability is found as $P_{\mathrm{D}}=Q_1\left(\sqrt{\lambda_t},\sqrt{2\Gamma^{-1}\left(1,P_{\mathrm{FA}}\right)}\right)$. Therefore, by noting that $\lambda_t=\left(Q_1^{-1}\left(P_{\mathrm{D}},\sqrt{2\Gamma^{-1}\left(1,P_{\mathrm{FA}}\right)}\right)\right)^2$, the statistics of the test formulated in (52) can be rewritten in terms of P_{D} and P_{FA} instead of λ_t by substituting $\lambda_t=\left(Q_1^{-1}\left(P_{\mathrm{D}},\sqrt{2\Gamma^{-1}\left(1,P_{\mathrm{FA}}\right)}\right)\right)^2$ in (52), and thus (53) and (64) can be also rewritten as functions of P_{D} and P_{FA}. Subsequently, all KLD equations in Sec. V.A and Sec. V.B can be rewritten in terms of $\{P_{\mathrm{D}},P_{\mathrm{FA}}\}$.

VI. KLD for Multi-user Multi-target ISAC System

The KLD measures in the previous section have been evaluated for a single user and a single target scenario. In this section, the weighted sum method is employed to evaluate KLD for multiple CUEs and targets scenario. Accordingly, the weighted sum for the KLD of each of the subsystems $\mathrm{s}\in\{\mathrm{ZF},\mathrm{MRT},\mathrm{rad}\}$ which consists of a number of CUEs or targets denoted as $J\in\{K,T\}$ can be formulated as

$$\mathrm{KLD}_{\mathrm{s}}=\sum_{i=1}^{J}c_{\mathrm{s},i}\mathrm{KLD}_{i,\mathrm{s},\mathrm{avg}}, \quad (70)$$

where $\sum_{i=1}^{J}c_i=1$, and for equal weights of $c_i=\frac{1}{J}$, $\mathrm{KLD}_{\mathrm{s}}$ is reduced to

$$\mathrm{KLD}_{\mathrm{s}}=\frac{1}{J}\sum_{i=1}^{J}\mathrm{KLD}_{i,\mathrm{s},\mathrm{avg}}. \quad (71)$$

On the other hand, for an ISAC system with multiple CUEs and multiple targets, we introduce a novel performance measure referred to the weighted sum of the relative entropy (WSRE). This performance measure will be very beneficial for ISAC systems as it can be employed to assess the performance of the system holistically as one entity rather than the conventional ways which typically characterize the ISAC system as two distinct subsystems. Additionally, WSRE will be very useful for a system designer to allocate the resources of BS, for example, power and antenna allocation. For a number of K CUEs and a number of T targets, WSRE is defined as

$$\mathrm{WSRE}_{\mathrm{ISAC}}\triangleq\sum_{k=1}^{K}c_{k,\mathrm{com}}\mathrm{KLD}_{k,\mathrm{com},\mathrm{avg}}+\sum_{t=1}^{T}c_{t,\mathrm{rad}}\mathrm{KLD}_{t,\mathrm{rad}}, \quad (72)$$

where $\sum_{k=1}^{K}c_{k,\mathrm{com}}+\sum_{t=1}^{T}c_{t,\mathrm{rad}}=1$. It worth noting that $c_{k,\mathrm{com}}$ and $c_{t,\mathrm{rad}}\ \forall\{k,t\}$ are design parameters which can be chosen to give some priority for a certain subsystem, CUE or target. In some scenarios in which CUEs and targets have the equal priority, then $c_{k,\mathrm{com}}=c_{t,\mathrm{rad}}=\frac{1}{K+T}\forall\{k,t\}$. Therefore, WSRE is reduced to

$$\mathrm{WSRE}_{\mathrm{ISAC}}=\frac{1}{K+T}\left(\sum_{k=1}^{K}\mathrm{KLD}_{k,\mathrm{com},\mathrm{avg}}+\sum_{t=1}^{T}\mathrm{KLD}_{t,\mathrm{rad}}\right) \quad (73)$$

VII. Numerical Results

This section presents the measured performance of the ISAC system introduced in this paper, which considers a multi-antenna BS that simultaneously transmits data symbols to K CUEs and aims at detecting a number of T targets. Monte Carlo simulation with 10^6 realizations for each run is used to generate the simulation (Sim.) results and the derived formulas in this paper are used to generate the theoretical performance. Unless otherwise stated, a number of 2 CUEs and a single target scenario, a number of $L=100$ snapshots, the antenna spacing is half the wavelength, i.e., $\Delta=0.5\lambda_0$, and the total transmit power is normalized to unity, i.e., $P_{\mathrm{T}}=1$, are considered. The total transmit power P_{T} is distributed among both subsystems with $P_{\mathrm{C}}=P_{\mathrm{T}}-P_{\mathrm{rad}}$ is the power allocated to the communication subsystem, where P_{rad} is the allocated power for the radar subsystem. For Figs. 3, 4, 5, 6, a single target located at $\theta=35^o$ is deployed in the environment, the radar covariance matrix is $\mathbf{R}_s=\mathbf{I}_{N_R}$, and the radar channel pathloss is normalized, i.e., $\alpha_{\mathrm{rad}}=1$. On the other hand, a number of $T=3$ targets with $\{\theta_1,\theta_2,\theta_3\}=\{35^o,100^o,160^o\}$ and $\{\alpha_{\mathrm{rad},1},\alpha_{\mathrm{rad},2},\alpha_{\mathrm{rad},3}\}=\{1,0.6,0.3\}$, in addition to a number of $K=3$ CUEs are considered in Fig. 7.

Fig. 3 presents the impact of the interference caused from radar subsystem on CUEs and the effect of estimation errors in $\mathbf{G}_{\mathrm{rad}}$ on the detection capability of the radar receiver, where the error in $\mathbf{G}_{\mathrm{rad}}$ is modeled using the variance of channel estimator σ_{err}^2. The total number of BS antennas is 20 which are distributed evenly among the radar and communication subsystems with QPSK signalling employed to modulate CUEs data symbols. The power allocated for radar and communication services are $P_{\mathrm{rad}}=0.1$ and $P_{\mathrm{C}}=0.9$ unit power, respectively. Moreover, the achievable performance using IMZF precoding is compared with IVMRT scheme. The simulation results confirm the accuracy of the derived equations in this paper for $\mathrm{KLD}_{\mathrm{IZF}}$, $\mathrm{KLD}_{\mathrm{IVMRT}}$, P_e and $\mathrm{KLD}_{\mathrm{rad}}$. As can be depicted from the figure, the interference caused from a subsystem to

the other limits the performance. For example, Fig. 3 a) shows that the probability of error for CUEs with IMZF precoding suffers from an error floor at 5×10^{-6} approximately, and $\mathrm{KLD}_{\mathrm{IZF}}$ also reaches an upper bound of about 54 bits for $\frac{P_{\mathrm{T}}}{\sigma_n^2} \gtrsim 30$ dB. On the other hand, the error floor for IVMRT scheme is $\sim 3 \times 10^{-4}$, and the upper bound of $\mathrm{KLD}_{\mathrm{IVMRT}}$ is almost 10 bits which is reached at $\frac{P_{\mathrm{T}}}{\sigma_n^2} \approx 20$ dB. The superiority of IMZF over IVMRT can be attributed to the fact that MRT generally suffers from inter-user-interference in addition to the interference caused by radar, and thus the total amount of interference a communication user suffers is much larger in MRT based precoding systems. As can be observed from Fig. 3 a), the detection capability of a communication system can be interpreted using KLD. More precisely, the relative entropy, or the KLD measure, is inversely proportional to SER where higher KLD values imply lower SER and thus better detection performance. It is worth noting that there is only one curve for each performance measure in Fig. 3 a) because a fixed $P_{\mathrm{C}} = 0.9$ is considered in this figure and the communication subsystem is independent of σ_{err}^2. It can be also seen from Fig. 3 b) and Fig. 3 c) that the channel estimation errors in $\mathbf{G}_{\mathrm{rad}}$ have a severe effect on the performance of the radar subsystem as the detection probability and KLD significantly decrease as σ_{err}^2 increases. For example, asymptotic detection probabilities of 0.2 and 0.7 are obtained when $\sigma_{\mathrm{err}}^2 = 0.1$ and 0.05, respectively, and KLD of about 3.45 and 11.56 bits for the same values of σ_{err}^2. However, although further decrease in σ_{err}^2 results in huge enhancement for $\mathrm{KLD}_{\mathrm{rad}}$, the improvement in P_{D} is small, for example, a decrease in σ_{err}^2 from 0.01 to 0.004 improves $\mathrm{KLD}_{\mathrm{rad}}$ from 63 to 143 bits at $\frac{P_{\mathrm{T}}}{\sigma_n^2} = 30$ dB, but the improvement in P_D is almost negligible at the same $\frac{P_{\mathrm{T}}}{\sigma_n^2}$. Interestingly, by comparing Fig. 3 b) with Fig. 3 c), it can be observed that the change in the detection probability is very slow as $\frac{P_{\mathrm{T}}}{\sigma_n^2}$ goes beyond 25 dB unlike KLD that has faster growing rate, which can be attributed to the fact that the detection probability is upper bounded by 1 whereas KLD is not upper bounded.

Figs. 4 and 5 show the performance of ISAC system with IMZF data precoder for different values of P_{rad}, where σ_{err}^2 is fixed at 0.01. All other system parameters considered for the simulation environment of these figures are similar to Fig. 3. It worth noting that different P_{rad} values impose different interference levels at CUEs, as well as, higher P_{rad} implies that less power is allocated to communication service since the total power is fixed. It is clear from these figures that the theoretical analysis agrees with the simulation results. Additionally, it can observed from Fig. 4 that increasing the value of P_{rad} can significantly degrade the performance of the communication subsystem by increasing SER and decreasing $\mathrm{KLD}_{\mathrm{IZF}}$. According the results in Fig. 4 a), an error floor for SER is obtained even with small amounts of P_{rad}, for example, the error floor is about 5×10^{-6} and substantially increases considerably as P_{rad} increases, for example, the error floor is more that 4.5×10^{-3} when $P_{\mathrm{rad}} \geq 0.3$ unit power. Similarly, Fig. 4 b) shows that $\mathrm{KLD}_{\mathrm{IZF}}$ goes below 15 bits for $P_{\mathrm{rad}} \geq 0.3$ regardless the increase in SNR.

On the other hand, it can be noticed from Fig. 5 that increasing P_{rad} can boost the detection capabilities of the radar subsystem by enhancing $\mathrm{KLD}_{\mathrm{rad}}$. For example, the upper bound of $\mathrm{KLD}_{\mathrm{rad}}$ with $P_{\mathrm{rad}} = 0.3$ is about 290 bits, whereas it is 70 and 164 for $P_{\mathrm{rad}} = 0.1$ and $P_{\mathrm{rad}} = 0.2$, respectively.

Fig. 6 shows the theoretical detection performance of the communication subsystem against the detection capability of the radar subsystem. Several values for $\frac{P_{\mathrm{T}}}{\sigma_n^2}$, $\frac{P_{\mathrm{T}}}{\sigma_n^2} = \{0, 5, 10, 15, 20\}$ dB, a number of $N = 50$ antennas distributed evenly among both subsystems with 25 antennas each, QPSK signalling for the communication part, and a channel estimator variance of $\sigma_{\mathrm{err}} = 0.01$ are considered in this figure. The amount of power allocated for the radar is varied over $0 < P_{\mathrm{rad}} < 1$, and then the pairs (P_e, P_D) and $(\mathrm{KLD}_{\mathrm{rad}}, \mathrm{KLD}_{\mathrm{IZF}})$ are calculated accordingly. As can be observed from Fig. 6 a), both systems suffer from poor detection capabilities regardless the power allocation at $\frac{P_{\mathrm{T}}}{\sigma_n^2} = 0$ dB. The best P_e can be obtained at this SNR level is about 10^{-3} that is obtained at $P_D = 0$, whereas the highest P_D is $\lesssim 0.8$ which occurs at $P_e \approx 1$. In terms of KLD, it can be seen from Fig. 6 b) that a $\mathrm{KLD}_{\mathrm{IZF}}$ of 16 bits is obtained at $\mathrm{KLD}_{\mathrm{rad}} = 0$ and a $\mathrm{KLD}_{\mathrm{rad}}$ of 13.2 bits is obtained when $\mathrm{KLD}_{\mathrm{IZF}} = 0$ at $\frac{P_{\mathrm{T}}}{\sigma_n^2} = 0$ dB. On the other hand, at mid-range SNR, $\frac{P_{\mathrm{T}}}{\sigma_n^2} = 5$ dB, the capability of the ISAC system in whole starts improving, however, only one of the two subsystems can operate efficiently at this range of SNR. For example, Fig. 6 a) depicts that $P_e > 10^{-3}$ is obtained for $P_D > 0.75$ when $\frac{P_{\mathrm{T}}}{\sigma_n^2} = 5$ dB, as well as Fig. 6 b) shows that the highest KLD obtained for each subsystem is about 50 bits which occurs when the KLD of the other system is 0 bit at the same value of $\frac{P_{\mathrm{T}}}{\sigma_n^2}$. Nonetheless, the detection capability of both systems is superior when $\frac{P_{\mathrm{T}}}{\sigma_n^2} \geq 10$ dB as a detection probability of $P_D \to 1$ can be obtained while maintaining low values for P_e if the value of P_{rad} is properly selected. On the other side, it is clear from Fig. 6 b) that a maximum KLD value of about 150 bits can be achieved for each subsystem when $\frac{P_{\mathrm{T}}}{\sigma_n^2} = 10$ dB. To investigate the trade-off of the KLD of the two subsystems at a fixed transmit SNR, let us consider the case of $\frac{P_{\mathrm{T}}}{\sigma_n^2} = 10$ dB. As can be observed from the figure, as one of the KLDs improves, the other one becomes worse. For example, the maximum achievable KLD for each subsystem is about 150 bits which occurs when the KLD of the other subsystem deteriorates to 0.

Fig. 7 presents a three dimensional (3D) plot for P_e in (36), $\mathrm{KLD}_{\mathrm{IZF}}$ in (71), P_{D} in (68), $\mathrm{KLD}_{\mathrm{rad}}$ in (71) and $\mathrm{WSRE}_{\mathrm{ISAC}}$ in (73) vs. P_{rad} and the number of allocated antennas to the radar subsystem, N_R. For this figure, three CUEs denoted as $\mathcal{U}_1$, $\mathcal{U}_2$ and $\mathcal{U}_3$ using BPSK, QPSK and 8PSK, respectively, and three targets denoted as $\mathcal{T}_1$, $\mathcal{T}_2$ and $\mathcal{T}_3$ with $\{\theta_1, \theta_2, \theta_3\} = \{35^o, 100^o, 160^o\}$ and $\{\alpha_{\mathrm{rad},1}, \alpha_{\mathrm{rad},2}, \alpha_{\mathrm{rad},3}\} = \{1, 0.6, 0.3\}$, are used. The values of $\frac{P_{\mathrm{T}}}{\sigma_n^2}$ and σ_{err}^2 are fixed at 10 dB and 0.01, respectively, the total number of BS antennas is fixed at $N = 50$, and N_R ranges from 1 to 49 with $N_C = N - N_R$. As can be observed from Fig. 7 a) and Fig. 7 b), SER and $\mathrm{KLD}_{\mathrm{IZF}}$ degrade as P_{rad} and/or N_R increase as the resources allocated for the communication subsystem are reduced. Moreover, it can be seen from these two subplots that as the modulation order increases the performance of CUE becomes worse as

This article has been accepted for publication in IEEE Transactions on Wireless Communications. This is the author's version which has not been fully edited and content may change prior to final publication. Citation information: DOI 10.1109/TWC.2023.3270390

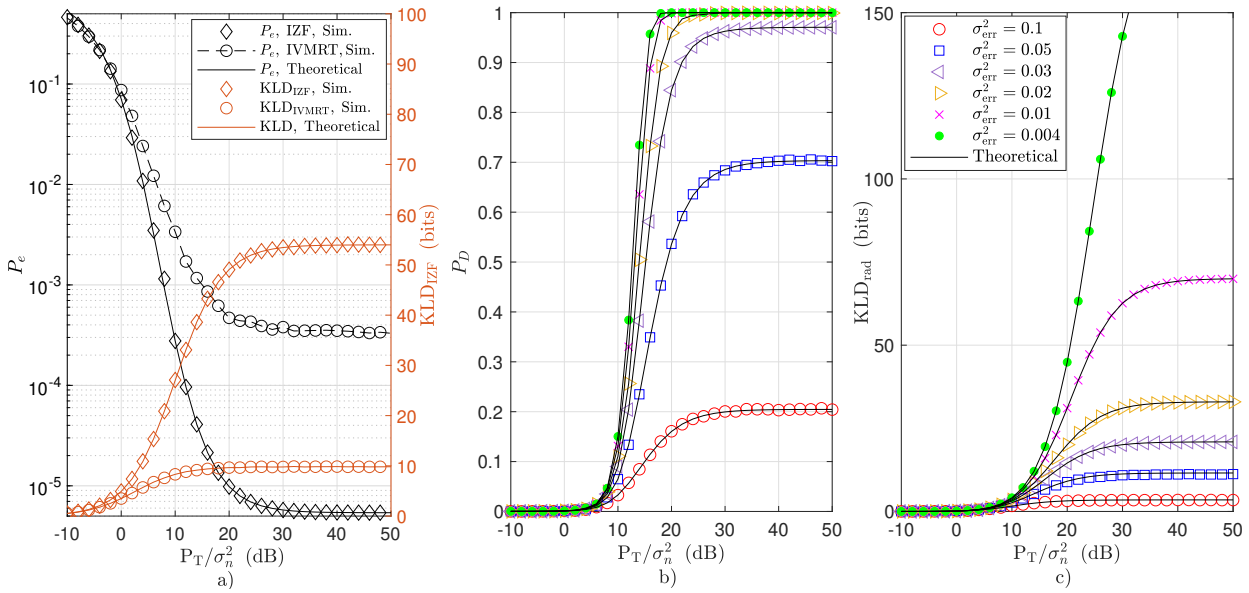

Fig. 3. The impact of radar-to-CUs interference and the estimation errors in $\mathbf{G}_{\mathrm{rad}}$ on the performance of CUs and radar subsystem, respectively, vs. the transmit SNR P_T/σ_n^2: a) The error rate and KLD of CUs, b) The detection probability P_{D} for the radar subsystem, and c) The KLD for the radar subsystems.

SER increases and KLD decreases. On the other hand, P_{D} and $\mathrm{KLD}_{\mathrm{rad}}$ improve as P_{rad} and/or N_R increase which can be clearly seen in Fig. 7 c) and Fig. 7 d). In addition, it can be also observed that the detection capability of BS substantially decreases as α_t decreases, which represents the radar cross section (RCS) of the target and the pathloss, i.e., lower α_t implies lower RCS and/or farther target. Fig. 7 e) presents a 3D plot for the weighted sum of KLD for both radar and communication subsystems, $\mathrm{WSRE}_{\mathrm{ISAC}}$ in (73). As can be clearly observed from this subplot, there is a trade-off between the performance of the radar and the communication subsystems. For example, it can be seen from Fig. 7 e) that there are two local maximum points: $(P_{\mathrm{rad}}, N_R, \mathrm{KLD}_{\mathrm{WSUM}}) \rightarrow (0, 1, 116)$ which represents the best scenario for the CUEs, and $(P_{\mathrm{rad}}, N_R, \mathrm{WSRE}_{\mathrm{ISAC}}) \rightarrow (1, 49, 20)$ which is the best case for the radar subsystem. Although the first scenario provides the global maximum $\mathrm{WSRE}_{\mathrm{ISAC}}$, it deteriorates the performance of the radar subsystem. On the other hand, by referring to Fig. 7 a) and Fig. 7 c), it can be realized that the SER of CUEs at $(P_{\mathrm{rad}}, N_R) \rightarrow (1, 49)$ is almost 1 and the detection probability for the radar subsystem is $P_{\mathrm{D}} = 1$. Fig. 7 f) shows the trade-off between $\mathrm{KLD}_{\mathrm{rad}}$ and $\mathrm{KLD}_{\mathrm{IZF}}$ as evaluated using (71) for different values of N_R, where the total number of antennas is fixed at $N = 50$. It is worth noting that the total power consumption is fixed for all the results in this figure, i.e., $\frac{P_{\mathrm{T}}}{\sigma_n^2} = 10$ dB, where the portion of power allocated for each subsystem is changed from 0% to 100% to get this trade-off. As can be noticed, for low values of $\mathrm{KLD}_{\mathrm{rad}}$, which basically occurs when the allocated P_{rad} is very low, $\mathrm{KLD}_{\mathrm{IZF}}$ is significantly high and increases as N_R decreases. By considering a fixed N_R value, it can be noticed that as P_{rad} increases, $\mathrm{KLD}_{\mathrm{IZF}}$ exponentially decays until reaching very low values. It is worth noting that the intersection between different curves with different N_R is due to different P_{rad} values. For example, the intersection between the two curves associated with $N_R = 20$ and $N_R = 30$ (e.g. the black-circles line and magenta dashed line) at $(\mathrm{KLD}_{\mathrm{rad}}, \mathrm{KLD}_{\mathrm{IZF}}) = (10, 6.2)$ occurs when the portion of the power allocated to the radar subsystem is 51% and 66% for the cases of $N_R = 30$ and $N_R = 20$, respectively. In other words, an ISAC system with $N_R = 30$ and 51% allocated power for the radar subsystem will provide the same KLD as $N_R = 20$ with 66% allocated radar power.

VIII. Conclusion

An ISAC system which consists of a multi-antenna BS serving CUEs and aims at detecting multiple targets simultaneously was introduced in this paper, where the separated deployment was considered. In addition, ZF and MRT were employed to precode the communication signals. The relative entropy or KLD was derived for both radar and communication subsystems, and a unified performance measure using the sum of weighted KLDs was proposed. In addition, the interference caused by the radar subsystem on CUEs and the impact of imperfect IC on the radar subsystem were analyzed and studied. Moreover, the relation between this performance measure from one side, and SER and detection probability on the other side was investigated. The obtained simulation results confirmed the derived equations where a perfect match was obtained. In addition, the results showed that there is a trade-off between the radar and the communication subsystems where enhancing one negatively impacts the other. Consequently, the system designer should be aware of this trade-off and allocate the power and antenna resources to maximize $\mathrm{WSRE}_{\mathrm{ISAC}}$ under some constraints on $\mathrm{KLD}_{\mathrm{IZF}}$ and $\mathrm{KLD}_{\mathrm{rad}}$ to guarantee boosting the performance of the whole system in an efficient way. Moreover, it was revealed that the effect of system imperfections, i.e., interference and imperfect channel estimation for $\mathbf{G}_{\mathrm{rad}}$, result

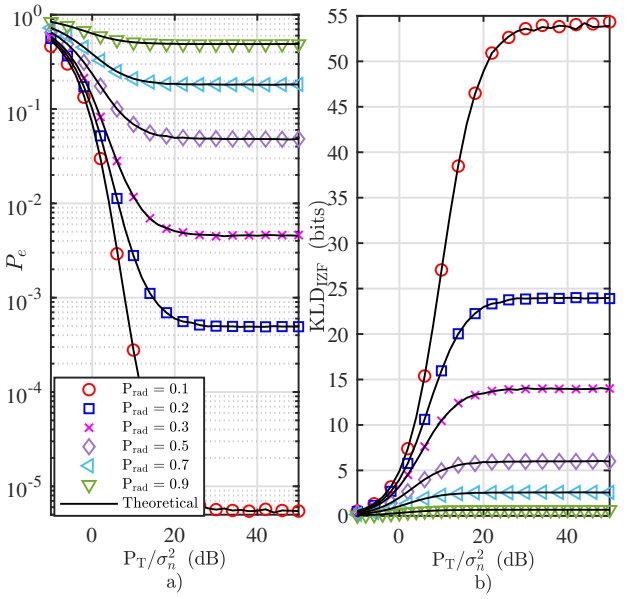

Fig. 4. The impact of different interference levels on the CUs represented by several values of P_{rad} and plotted vs. the transmit SNR P_T/σ_n^2, where $N = 20$ with $\{N_R, N_C\} = \{10, 10\}$: a) The probability of symbols errors, and b) The KLD for CUs.

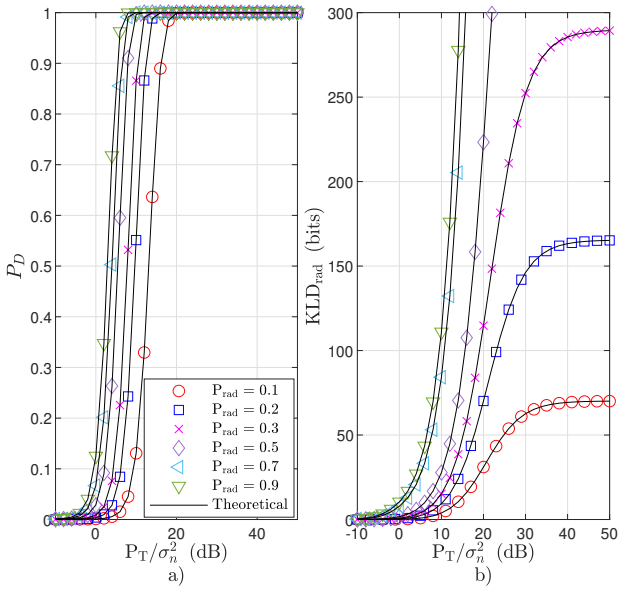

Fig. 5. The performance of the radar system vs. the transmit SNR P_T/σ_n^2 with $\sigma_{\mathrm{err}}^2 = 0.01$ and several values of P_{rad}, where $N = 20$ with $\{N_R, N_C\} = \{10, 10\}$: a) The probability of detection, and b) The KLD for radar subsystem.

in an error floor in SER and upper bound in P_{D}, $\mathrm{KLD_{IZF}}$ and $\mathrm{KLD_{rad}}$. It was also disclosed that MRT based precoding could experience a considerable error floor due to inter-user-interference resulted from MRT, in addition to the interference caused by the radar subsystem.

Future work may include using the derived KLD to allocate the BS resources among the users and targets to maximize $\mathrm{WSRE_{ISAC}}$ for given constraints on individual KLDs. Moreover, the employment of KLD for the analysis, design and optimization of ISAC systems in which the radar subsystem

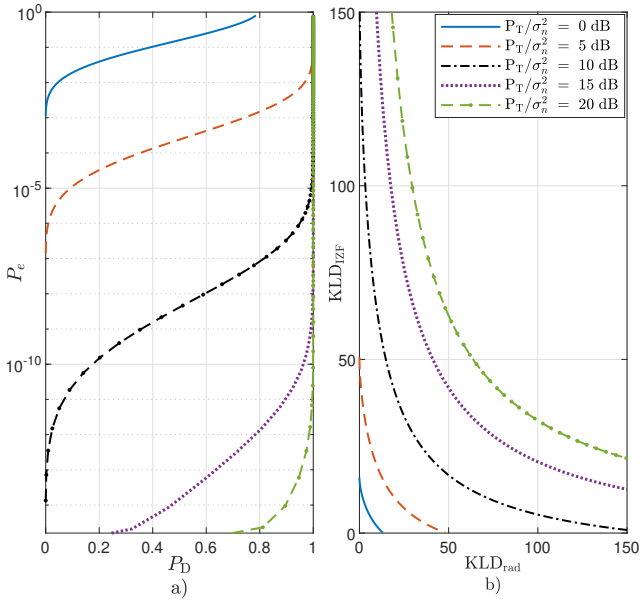

Fig. 6. The trade-off between the radar and communication subsystems for different values of the transmit SNR $P_{\mathrm{T}}/\sigma_n^2$, where $N = 50$ with $\{N_R, N_C\} = \{25, 25\}$: a) The tradeoff between P_e and P_{D}, and b) The trade-off between $\mathrm{KLD_{IZF}}$ and $\mathrm{KLD_{rad}}$.

aims at estimating the targets' parameters is also an interesting research topic.

IX. Appendix

A. *Appendix* I

Central Limit Theorem (CLT) is applied to approximate the distribution of $t_{k,i} = \sum_{n_c=1}^{N_C} d_i[l]\,\mathbf{g}_k^T(n_c)\,\mathbf{g}_i^*(n_c)\,\forall i \neq k$ for considerable values of N_C. Therefore, with a normalized signal constellation, $\mathbb{E}\left[|d_i[l]|^2\right] = 1$, $t_{k,i} \sim \mathcal{CN}\left(0, 2\sigma_t^2\right)$ with $\sigma_t^2 = 2\sigma_g^4 N_C$. On the other hand, the exact density function of $z_i = \|\mathbf{g}_i\|^2$ is Chi distribution, which can be derived as below. Let us express z_i as $z_i = \sqrt{\sum_{n_c=1}^{N_C} |\mathbf{g}_i(n_c)|^2}$, which can be rewritten as $z_i = \sigma_g \tilde{z}_i$ where $\tilde{z}_i = \sqrt{\sum_{n_c=1}^{N_C} \left(\frac{\mathbf{g}_{i,\Re}(n_c)}{\sigma_g}\right)^2 + \left(\frac{\mathbf{g}_{i,\Im}(n_c)}{\sigma_g}\right)^2}$. Thereafter, by using the definition of a Chi distributed random variable, it can be easily shown that $\tilde{z}_i \sim \mathrm{Chi}(2N_C)$ with PDF given by

$$f_{\tilde{z}_i}(\tilde{z}_i) = \frac{1}{2^{N_C-1}\Gamma(N_C)} \tilde{z}_i^{2N_C-1} \mathrm{e}^{-\frac{1}{2}\tilde{z}_i^2}, \tag{74}$$

and then by employing random variable transformation, it can be found that $z_i \triangleq \sigma_g \tilde{z}_i$ is also Chi distributed with PDF given by

$$f_{z_i}(z_i) = \frac{1}{2^{N_C-1}\Gamma(N_C)\,\sigma_g^{2N_C}} z_i^{2N_C-1} \mathrm{e}^{-\frac{1}{2\sigma_g^2} z_i^2}. \tag{75}$$

The ratio distribution of independent Gaussian and Chi random variables is a Student-t distribution. However, the analysis for the density of a sum of K Student-t random variables is not tractable. Therefore, to make the analysis tractable, we use the fact that for large value of

This article has been accepted for publication in IEEE Transactions on Wireless Communications. This is the author's version which has not been fully edited and content may change prior to final publication. Citation information: DOI 10.1109/TWC.2023.3270390

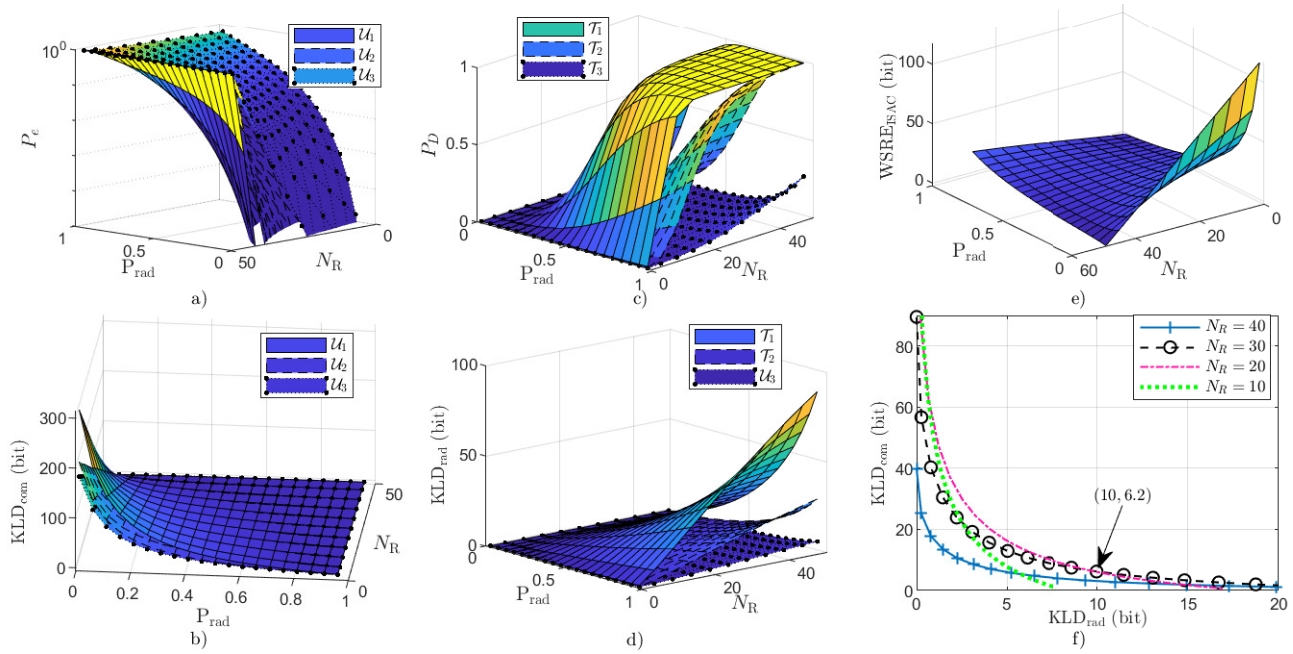

Fig. 7. A 3D plot for the KLD of ISAC system vs. N_R and P_{rad} where $N = 50$: a) The symbol error rate of CUEs, b) The KLD of CUEs, c) The detection probability P_{D} of the radar subsystem, d) The KLD of the radar subsystem, e) The $\mathrm{WSRE_{ISAC}}$ of ISAC system, and f) The $\mathrm{WSRE_{ISAC}}$ of ISAC system viewed from different angle.

the degrees of freedom of Chi distribution, which is directly proportional to N_C, the Chi density function can be approximated as real positive Gaussian PDF, i.e., $z_i \sim \mathcal{N}\left(\sigma_g\sqrt{2}\frac{\Gamma(0.5(2N_C+1))}{\Gamma(N_C)}, \left(2N_C - 2\left(\frac{\Gamma(0.5(2N_C+1))}{\Gamma(N_C)}\right)^2\right)\sigma_g^2\right)$. It is worthy noting that the assumption of large N_C is reasonable in multi-user MIMO systems since BS is typically equipped with a large number of antennas. Thereafter, we check the correlation between $t_{k,i}$ and z_i. To begin, the correlation between $t_{k,i}$ and z_i^2 is checked because it is more traceable.

$$\rho_{t_i,z_i^2} = \frac{\mathbb{E}\left[\left(t_{k,i} - \mu_{t_{k,i}}\right)\left(z_i^2 - \mu_{z_i^2}\right)\right]}{\sqrt{\mathrm{var}\left[t_{k,i}\right]\mathrm{var}\left[z_i^2\right]}}. \tag{76}$$

By noting that $\mu_{t_{k,i}} = 0$, and then substituting for z_i and $t_{k,i}$ and using the fact that the expectation operator can be distributed over summation and over a product of independent random variables, ρ_{t_i,z_i^2} can be found as

$$\rho_{t_i,z_i^2} = \frac{\sum_{n_{c1}=1}^{N_C}\sum_{n_{c2}=1}^{N_C}\mathbb{E}\left[\mathbf{g}_i^*(n_{c1})|\mathbf{g}_i(n_{c2})|^2\right]\mathbb{E}\left[\mathbf{g}_k^T(n_{c1})\right]}{\sqrt{\mathrm{var}\left[t_{k,i}\right]\mathrm{var}\left[z_i\right]}} = 0, \tag{77}$$

where the last equality holds as $\mathbf{g}_i$ and $\mathbf{g}_k$ are i.i.d for $i \neq k$ with zero mean (e.g. $\mathbb{E}\left[\mathbf{g}_k^T(n_{c1})\right] = 0$). Consequently, $t_{k,i}$ and z_i are uncorrelated and approximately jointly Gaussian variables for considerable values of N_C, and thus it can be assumed that they are independent. Next, using the definition of $\tilde{v}_{k,i}$

$$\tilde{v}_{k,i} \triangleq \sqrt{P_{i,\mathrm{com}}}\frac{t_{k,i}}{z_i} = \sqrt{P_{i,\mathrm{com}}}\left(v_{k,i,\mathfrak{R}} + jv_{k,i,\mathfrak{R}}\right), \tag{78}$$

where the subscripts $(\cdot)_{\mathfrak{R}}$ and $(\cdot)_{\mathfrak{I}}$ denote the real and imaginary components of a complex number, respectively, $v_{k,i,\mathfrak{R}} = \frac{t_{k,i,\mathfrak{R}}}{z_i}$ and $v_{k,i,\mathfrak{I}} = \frac{t_{k,i,\mathfrak{I}}}{z_i}$. Since $t_{k,i}$ is $\mathcal{N}\left(0, 2\sigma_t^2\right)$ with identically distributed real and imaginary parts, then $t_{k,i,\mathfrak{R}}$ and $t_{k,i,\mathfrak{I}}$ are $\mathcal{N}\left(0,\sigma_t^2\right)$. When $\Pr\left(z_i > 0\right) \to 1$, or $\mu_{z_i} \gg \sigma_{z_i}$, which is a satisfied condition since z_i is a strictly positive random variable in our case, the cumulative distribution function (CDF) of the ratio of two normally distributed random variables, $v_{k,i,\mathfrak{R}} = \frac{t_{k,i,\mathfrak{R}}}{z_i}$, having means of $\mu_{t,\mathfrak{R}} = 0$ and $\mu_z = \sqrt{2}\frac{\Gamma(0.5(2N_C+1))}{\Gamma(N_C)}$, and unequal variance values of $\sigma_t^2 = 2\sigma_g^4 N_C$ and $\sigma_z^2 \triangleq 2N_C - 2\left(\frac{\Gamma(0.5(2N_C+1))}{\Gamma(N_C)}\right)^2$, can be approximated as [76, Eq. (5)],

$$F_{v_{k,i,\mathfrak{R}}}(v) = \Phi\left(\frac{\mu_z v}{\sigma_t\sigma_z\left(\frac{v^2}{\sigma_t^2} + \frac{1}{\sigma_z^2}\right)^{0.5}}\right), \tag{79}$$

where $\Phi(x) \triangleq \frac{1}{\sqrt{2\pi}}\int_{-\infty}^{x} \mathrm{e}^{-\frac{u^2}{2}}du$ is the CDF of a standard normal distribution, i.e., $\mathcal{N}(0,1)$. It is worthy to note that $v_{k,i,\mathfrak{I}}$ have the same CDF as $v_{k,i,\mathfrak{R}}$. Therefore, by using the derivative of $F_{v_{k,i,\mathfrak{R}}}(v)$, which can be solved using the chain rule and the derivative of $\Phi(x)$ as $\frac{\partial}{\partial v}\Phi(x) \triangleq \frac{1}{\sqrt{2\pi}}\mathrm{e}^{-\frac{x^2}{2}}$, the PDF can be found as (80) on page 17. Interestingly, for typical range of $N_C \gg 1$, $f_{v_{k,i,\mathfrak{R}}}(v)$ tends to take the shape of Gaussian random variable [76, Eq. (5)], consequently, $f_{v_{k,i,\mathfrak{R}}}(v)$ is assumed following $\mathcal{N}\left(\mu_v, \sigma_v^2\right)$ where

$$\mu_v \triangleq \mathbb{E}\left[v_{k,i,\mathfrak{R}}\right] = \mathbb{E}\left[t_{k,i,\mathfrak{R}}\right]\mathbb{E}\left[\frac{1}{z_i}\right] = 0, \tag{81}$$

and

$$\begin{aligned}\sigma_v^2 &\triangleq \mathbb{E}\left[\left(v_{k,i,\mathfrak{R}} - \mu_v\right)^2\right] = \mathbb{E}\left[\left(v_{k,i,\mathfrak{R}}\right)^2\right] \\ &= \mathbb{E}\left[t_{k,i,\mathfrak{R}}^2\right]\mathbb{E}\left[\frac{1}{z_i^2}\right] = \sigma_t^2\int_0^\infty \frac{1}{z_i^2}f_z(z)\,dz.\end{aligned} \tag{82}$$

By using the PDF $f_z(z)$ which has been derived in (75), σ_v^2 can be written as

$$f_{v_{k,i,\Re}}(v) \triangleq \frac{\partial}{\partial v} F_{v_{k,i,\Re}}(v) = \frac{\mu_z}{\sigma_t \sigma_z \sqrt{2\pi}} \left(\frac{v^2}{\sigma_t^2} + \frac{1}{\sigma_z^2}\right)^{-0.5} \left(1 - \frac{v^2}{\sigma_t^2}\left(\frac{v^2}{\sigma_t^2} + \frac{1}{\sigma_z^2}\right)^{-1}\right) \exp\left(-\frac{\mu_z^2 v^2}{2\sigma_z^2\left(v^2 + \frac{\sigma_t^2}{\sigma_z^2}\right)}\right). \quad (80)$$

$$\sigma_v^2 = \frac{\sigma_t^2}{2^{N_C-1}\Gamma(N_C)\,\sigma_g^{2N_C}} \int_0^\infty z_i^{2N_C-3} \mathrm{e}^{-\frac{1}{2\sigma_g^2} z_i^2} dz. \quad (83)$$

Thereafter, by employing integration by substitution rule with $y = \frac{1}{2\sigma_g^2} z_i^2$, the value of σ_v^2 can be found as $\sigma_v^2 = \sigma_g^2$. Therefore, $\tilde{v}_{k,i}$ can be approximated as a symmetric complex Gaussian random variable, i.e., $\tilde{v}_{k,i} \sim \mathcal{CN}\left(0, 2P_{i,\mathrm{com}}\sigma_v^2\right)$. Next, we check the correlation between $\tilde{v}_{k,i} \forall i \neq k$. It can be easily realized that $z_i = \|\mathbf{g}_i\| \,\forall i$ are independent, as well as, the correlation coefficient between $t_{k,i} \forall i \neq k$ can be found using similar derivations in (77) as

$$\rho_{i,j} = \frac{\mathbb{E}\left[t_{k,i} t_{k,j}^*\right]}{\sqrt{\mathrm{var}\left[t_{k,i}\right] \mathrm{var}\left[t_{k,j}\right]}} = \frac{\sum_{n_c=1}^{N_C}\sum_{n_c=1}^{N_C} \mathbb{E}[\mathbf{g}_i^*(n_c)]\mathbb{E}\left[|\mathbf{g}_k(n_c)|^2\right]\mathbb{E}\left[\mathbf{g}_j^*(n_c)\right]}{\sqrt{\mathrm{var}\left[t_{k,i}\right] \mathrm{var}\left[t_{k,j}\right]}} = 0. \quad (84)$$

Consequently, since $t_{k,i}$ is complex Gaussian distributed according to CLT and $\rho_{i,j} = 0 \forall i \neq j$ with approximately jointly Gaussian, $t_{k,i}$ and $t_{k,j}$ are independent for $i \neq j$. Moreover, since z_i and z_j are independent $\forall i \neq j$, and thus $\tilde{v}_{k,i} = \sqrt{P_{i,\mathrm{com}}} \frac{t_{k,i}}{z_i}$ and $\tilde{v}_{k,j} = \sqrt{P_{j,\mathrm{com}}} \frac{t_{k,j}}{z_j}$ for $i \neq j$ are also independent. Finally, $\omega_{\mathrm{MRT}} = \sum_{\substack{i=1 \\ i\neq k}}^{K} \tilde{v}_{k,i}$ is a sum of $K-1$ independent complex Gaussian random variables each of which $\tilde{v}_{k,i} \sim \mathcal{CN}\left(0, 2P_{i,\mathrm{com}}\sigma_v^2\right)$, thus $\omega_{\mathrm{MRT}} \sim \mathcal{CN}\left(0, 2\sigma_v^2 \sum_{\substack{i=1 \\ i\neq k}}^{K} P_{i,\mathrm{com}}\right)$. Therefore, the equivalent inter-user and radar interference plus noise $\tilde{\omega}_{\mathrm{MRT}} \sim \mathcal{CN}\left(0, 2\sigma_\omega^2\right)$ where $\sigma_\omega^2 = \sigma_v^2 \sum_{\substack{i=1 \\ i\neq k}}^{K} P_{i,\mathrm{com}} + \sigma_\eta^2$ with $\sigma_\eta^2 = P_{\mathrm{rad}}\sigma_f^2 + \sigma_n^2$.

B. Appendix II

Substituting the approximation given by (56) in (59) and then performing some mathematical manipulation including some logarithmic and exponential identities such as $\ln\left(\frac{x}{y}\right) = \ln x - \ln y$, $\ln(xy) = \ln x + \ln y$ and $\ln \mathrm{e}^x = x$ yield

$$\mathcal{I}_2 \approx \sqrt{\lambda_t}\mathcal{I}_{2a} - \left(\left(\frac{1}{2}\ln(2\pi) + \frac{1}{4}\ln(\lambda_t)\right)\mathcal{I}_{2b} + \frac{1}{4}\mathcal{I}_{2c}\right) + \mathcal{I}_{2d}, \quad (85)$$

where $\mathcal{I}_{2a}$, $\mathcal{I}_{2b}$, $\mathcal{I}_{2c}$ and $\mathcal{I}_{2d}$ are given in Table I.

Thereafter, by using integration by substitution with $y = \sqrt{\xi}$ and then using [77, Eq. 1.3.3.8, pp. 140], $\mathcal{I}_{2a}$ can be found as

$$\mathcal{I}_{2a} = -\sqrt{2\pi}\mathrm{erf}\left(\frac{1}{\sqrt{2\lambda_t}}\right) + \sqrt{2\pi} + \frac{2}{\sqrt[2\lambda_t]{\mathrm{e}}\sqrt{\lambda_t}}. \quad (86)$$

Moreover, using integration by parts rule with $dv = \mathrm{e}^{-0.5\xi}$ and $u = \ln(\xi)$ and then using the definition of the exponential integral, $\mathcal{I}_{2c}$ can be found as

$$\mathcal{I}_{2c} = \left(-\frac{2\ln\lambda_t}{\sqrt[2\lambda_t]{\mathrm{e}}} + 2\mathrm{Ei}_1\left(\frac{1}{2\lambda_t}\right)\right). \quad (87)$$

To solve $\mathcal{I}_{2d}$, let us consider the first five terms in the summation, i.e., $Q = 5$ which can provide a very good approximation for $\xi \geq \frac{1}{\lambda_t}$. In this case we obtain $\sum_{q=1}^{Q=5}(\cdot) < 1$, and thus Taylor series expansion can be adopted and the first term is sufficient for providing accurate results, i.e., $\ln\left(1 + \sum_{q=1}^{Q=5}(\cdot)\right) \approx \sum_{q=1}^{Q=5}(\cdot)$ for $\sum_{q=1}^{Q=5}(\cdot) < 1$. Thereafter, by using the fact that summation and integration are interchangeable operations, $\mathcal{I}_{2d}$ can be evaluated as [77, Eq. 1.3.2.4, pp. 137]

$$\mathcal{I}_{2d} = \sum_{q=1}^{Q=5} \frac{\prod_{k=1}^{q}\left[(2k-1)^2\right]}{q!8^q\lambda_t^{0.5q}} \frac{1}{0.5^{1-0.5q}}\Gamma\left(1-0.5q, \frac{0.5}{\lambda_t}\right), \quad (88)$$

where $\Gamma(\cdot,\cdot)$ is the upper incomplete gamma function.

C. Appendix III

By substituting the infinite series representation provided in (55) for the modified Bessel function in (67), $\mathcal{I}_{4a}$ can be given by

$$\mathcal{I}_{4a} = \int_0^{\frac{1}{\lambda_t}} \mathrm{e}^{-0.5\xi} \sum_{l_1=0}^{\infty} \frac{\lambda_t^{l_1}}{2^{2l_1}(l_1!)^2}\xi^{l_1} \ln\left(1 + \sum_{l_2=1}^{\infty} \frac{\lambda_t^{l_2}}{2^{2l_2}(l_2!)^2}\xi^{l_2}\right) d\xi. \quad (89)$$

After that, by noting that $\sum_{l_2=1}^{\infty} \frac{\lambda_t^{l_2}}{2^{2l_2}(l_2!)^2}\xi^{l_2} < 1$ for $0 \leq \xi < \frac{1}{\lambda_t}$, the first term of the Taylor series is considered to approximate the logarithmic function and then interchange the summations and integration order, $\mathcal{I}_{4a}$ can be accurately approximated as

$$\mathcal{I}_{4a} \approx \sum_{l_1=0}^{\infty} \frac{\lambda_t^{l_1}}{2^{2l_1}(l_1!)^2} \sum_{l_2=1}^{\infty} \frac{\lambda_t^{l_2}}{2^{2l_2}(l_2!)^2} \int_0^{\frac{1}{\lambda_t}} \mathrm{e}^{-0.5\xi}\xi^{l_1+l_2} d\xi, \quad (90)$$

which can be solved as

$$\mathcal{I}_{4a} \approx \sum_{l_1=0}^{\infty} \frac{\lambda_t^{l_1}}{2^{2l_1}(l_1!)^2} \sum_{l_2=1}^{\infty} \frac{\lambda_t^{l_2}}{2^{2l_2}(l_2!)^2} \frac{2^{1+0.5(l_1+l_2)}}{(1+l_1+l_2)\lambda_t^{0.5(l_1+l_2)}} \times \mathrm{e}^{-\frac{0.25}{\lambda_t}} \mathrm{M}_{0.5(l_1+l_2),0.5(l_1+l_2)+0.5}\left(\frac{0.5}{\lambda_t}\right). \quad (91)$$

On the other hand, by substituting the approximation in (56) to approximate $\mathcal{I}_{4b}$ given in (67) for $\xi > \frac{1}{\lambda_t}$ and using some algorithmic identities such as $\log\left(\frac{x}{y}\right) = \log x - \log y$, $\log(xy) = \log x + \log y$ and $\log(x^y) = y\log x$, then $\mathcal{I}_{4b}$ can be simplified to (93) and (93) on page 18, where $\mathcal{Q}_{\mathrm{sum},q} = \sum_{q=1}^{Q} \frac{1}{q_1!8^q\sqrt{\lambda_t^q}} \prod_{k=1}^{q}\left[(2k-1)^2\right] \forall q \in \{q_1, q_2\}$, and $\mathcal{I}_{4b,i} \forall i \in \{1, 2, \cdots, 8\}$ are given in Table II. Due to the limited space, we will show the complete solutions for $\mathcal{I}_{4b,1}$

This article has been accepted for publication in IEEE Transactions on Wireless Communications. This is the author's version which has not been fully edited and content may change prior to final publication. Citation information: DOI 10.1109/TWC.2023.3270390

TABLE I
THE VALUES OF I_{2a}, I_{2b},...,I_{2d} THAT ARE REQUIRED TO COMPUTE $\mathrm{KLD}(\xi_{H0}||\xi_{H1})$.

$\mathcal{I}_{2a}=\int_{\frac{1}{\lambda_t}}^{\infty}\sqrt{\xi}\mathrm{e}^{-0.5\xi}d\xi$	$\mathcal{I}_{2b}=\int_{\frac{1}{\lambda_t}}^{\infty}\mathrm{e}^{-0.5\xi}d\xi=\frac{2}{2\lambda_t\sqrt[4]{\mathrm{e}}}$	$\mathcal{I}_{2c}=\int_{\frac{1}{\lambda_t}}^{\infty}\mathrm{e}^{-0.5\xi}\ln(\xi)\,d\xi$
$\mathcal{I}_{2d}=\int_{\frac{1}{\lambda_t}}^{\infty}\mathrm{e}^{-0.5\xi}\ln\left(1+\sum_{q=1}^{Q}\left(\frac{1}{\left(\sqrt{\lambda_t\xi}\right)^q}\frac{\prod_{k=1}^{q}\left[(2k-1)^2\right]}{q!8^q}\right)\right)d\xi$		

$$\begin{aligned}\mathcal{I}_{4b}\approx\ & \int_{\frac{1}{\lambda_t}}^{\infty}\mathrm{e}^{-0.5\xi}\frac{\exp\left(\sqrt{\lambda_t\xi}\right)}{\sqrt{2\pi}\sqrt[4]{\lambda_t\xi}}\left(1+\sum_{q1=1}^{Q}\left(\frac{1}{\left(\sqrt{\lambda_t\xi}\right)^q}\frac{\prod_{k=1}^{q}\left[(2k-1)^2\right]}{q!8^q}\right)\right)\\ &\times\left(\sqrt{\lambda_t\xi}-\ln\left(\sqrt{2\pi}\sqrt[4]{\lambda_t}\right)-0.25\ln(\xi)+\ln\left(1+\sum_{q2=1}^{Q}\left(\frac{1}{\left(\sqrt{\lambda_t\xi}\right)^q}\frac{\prod_{k=1}^{q}\left[(2k-1)^2\right]}{q!8^q}\right)\right)\right)d\xi \qquad (92)\\ =\ & \frac{1}{\sqrt{2\pi}\sqrt[4]{\lambda_t}}\left(\sqrt{\lambda_t}\mathcal{I}_{4b,1}-\ln\left(\sqrt{2\pi}\sqrt[4]{\lambda_t}\right)\mathcal{I}_{4b,2}-0.25\mathcal{I}_{4b,3}+\mathcal{Q}_{\mathrm{sum},q_2}\mathcal{I}_{4b,4}\right.\\ &\left.+\mathcal{Q}_{\mathrm{sum},q_1}\left(\sqrt{\lambda_t}\mathcal{I}_{4b,5}-\ln\left(\sqrt{2\pi}\sqrt[4]{\lambda_t}\right)\mathcal{I}_{4b,6}-0.25\mathcal{I}_{4b,7}+\mathcal{Q}_{\mathrm{sum},q_2}\mathcal{I}_{4b,8}\right)\right), \qquad (93)\end{aligned}$$

TABLE II
THE VALUES OF $I_{4b,1}$, $I_{4b,2}$,...,$I_{4b,8}$ THAT ARE REQUIRED TO COMPUTE $\mathrm{KLD}(\xi_{H1}||\xi_{H0})$.

$\mathcal{I}_{4b,1}=\int_{\frac{1}{\lambda_t}}^{\infty}\xi^{0.25}\exp\left(-0.5\xi+\sqrt{\lambda_t\xi}\right)d\xi$	$\mathcal{I}_{4b,2}=\int_{\frac{1}{\lambda_t}}^{\infty}\xi^{-0.25}\exp\left(-0.5\xi+\sqrt{\lambda_t\xi}\right)d\xi$
$\mathcal{I}_{4b,3}=\int_{\frac{1}{\lambda_t}}^{\infty}\xi^{-0.25}\ln(\xi)\exp\left(-0.5\xi+\sqrt{\lambda_t\xi}\right)d\xi$	$\mathcal{I}_{4b,4}=\int_{\frac{1}{\lambda_t}}^{\infty}\frac{1}{\xi^{\frac{q_2}{2}+\frac{1}{4}}}\exp\left(-0.5\xi+\sqrt{\lambda_t\xi}\right)d\xi$
$\mathcal{I}_{4b,5}=\int_{\frac{1}{\lambda_t}}^{\infty}\frac{1}{\xi^{\frac{q_1}{2}-\frac{1}{4}}}\exp\left(-0.5\xi+\sqrt{\lambda_t\xi}\right)d\xi$	$\mathcal{I}_{4b,6}=\int_{\frac{1}{\lambda_t}}^{\infty}\frac{1}{\xi^{\frac{q_1}{2}+\frac{1}{4}}}\exp\left(-0.5\xi+\sqrt{\lambda_t\xi}\right)d\xi$
$\mathcal{I}_{4b,7}=\int_{\frac{1}{\lambda_t}}^{\infty}\frac{1}{\xi^{\frac{q_1}{2}+\frac{1}{4}}}\ln(\xi)\exp\left(-0.5\xi+\sqrt{\lambda_t\xi}\right)d\xi$	$\mathcal{I}_{4b,8}=\int_{\frac{1}{\lambda_t}}^{\infty}\frac{1}{\xi^{\frac{q_1}{2}+\frac{q_2}{2}+\frac{1}{4}}}\exp\left(-0.5\xi+\sqrt{\lambda_t\xi}\right)d\xi$

and $\mathcal{I}_{4b,3}$ only, anyway, the other integrals can be solved in a similar way. By using integration by substitution rule with $y=\sqrt{0.5\xi}$ followed by the complete square rule to write the exponents in a more convenient form, i.e., the integrand is multiplied by $\exp(\pm\lambda_t/2)$, $\mathcal{I}_{4b,1}$ and $\mathcal{I}_{4b,3}$ can be expressed as

$$\mathcal{I}_{4b,1}=4\,(2)^{0.25}\exp\left(\frac{\lambda_t}{2}\right)\int_{\sqrt{\frac{1}{2\lambda_t}}}^{\infty}y^{1.5}\exp\left(-\left(y-\sqrt{\frac{\lambda_t}{2}}\right)^2\right)dy, \qquad (94)$$

$$\mathcal{I}_{4b,3}=4(2)^{-0.25}\exp\left(\frac{\lambda_t}{2}\right)\int_{\sqrt{\frac{1}{2\lambda_t}}}^{\infty}y^{0.5}\ln\left(2y^2\right)\exp\left(-\left(y-\sqrt{\frac{\lambda_t}{2}}\right)^2\right)dy. \qquad (95)$$

Next, with the aid of the series representation of $\exp\left(-x^2\right)$ [75, Eq. 1.211.3, pp. 26] and then interchanging the integration and summation operations, $\mathcal{I}_{4b,1}$ and $\mathcal{I}_{4b,3}$ can be simplified to

$$\mathcal{I}_{4b,1}=4\,(2)^{0.25}\exp\left(\frac{\lambda_t}{2}\right)\sum_{k=0}^{\infty}\frac{(-1)^k}{k!}\int_{\sqrt{\frac{1}{2\lambda_t}}}^{\infty}y^{1.5}\sum_{l=0}^{\infty}\left(y-\sqrt{\frac{\lambda_t}{2}}\right)^{2k}dy, \qquad (96)$$

$$\mathcal{I}_{4b,3}=4\,(2)^{-0.25}\exp\left(\frac{\lambda_t}{2}\right)\sum_{k=0}^{\infty}\frac{(-1)^k}{k!}\int_{\sqrt{\frac{1}{2\lambda_t}}}^{\infty}y^{0.5}\ln\left(2y^2\right)\times\left(y-\sqrt{\frac{\lambda_t}{2}}\right)^{2k}dy. \qquad (97)$$

Thereafter, the binomial expansion theorem is invoked and interchanging the summation and integration is applied. Additionally, to make the series converges to the answer quickly, we limit the integration to an upper bound of $y_{\mathrm{U}}=\sqrt{\lambda_t/2}+4/\sqrt{2}$ instead of ∞ as $\exp\left(-\left(y-\sqrt{\lambda_t/2}\right)^2\right)\approx 0$ for $y>\sqrt{\lambda_t/2}+4/\sqrt{2}$. It is worthy to notice that the exponential term has a form similar to a normal distribution with a mean of $\mu=\sqrt{\lambda_t/2}$ and a standard deviation of $\sigma=1/\sqrt{2}$, and thus it can interpreted that more than 99.9999% of the area under the curve is in the range $\mu-4\sigma\leq y\leq\mu+4\sigma$. Subsequently, $\mathcal{I}_{4b,1}$ can be evaluated as

$$\mathcal{I}_{4b,1} = 4\,(2)^{0.25} \exp\left(\frac{\lambda_t}{2}\right) \sum_{k=0}^{\infty} \frac{(-1)^k}{k!} \sum_{l=0}^{2k} (-1)^{2k-l} \binom{2k}{l} \times \left(\frac{\lambda_t}{2}\right)^{0.5(2k-l)} \int_{\sqrt{\frac{1}{2\lambda_t}}}^{y_{\mathrm{U}}} y^{l+1.5} dy$$

$$= 4\,(2)^{0.25} \exp\left(\frac{\lambda_t}{2}\right) \sum_{k=0}^{\infty} \frac{(-1)^k}{k!} \sum_{l=0}^{2k} (-1)^{2k-l} \binom{2k}{l} \times \left(\frac{\lambda_t}{2}\right)^{0.5(2k-l)} \frac{1}{l+2.5} \left(y_{\mathrm{U}}^{l+2.5} - \left(\frac{1}{2\lambda_t}\right)^{\frac{l+2.5}{2}}\right), \quad (98)$$

and $\mathcal{I}_{4b,3}$ can be further simplified to

$$\mathcal{I}_{4b,3} = 4\,(2)^{-0.25} \exp\left(\frac{\lambda_t}{2}\right) \sum_{k=0}^{\infty} \frac{(-1)^k}{k!} \sum_{l=0}^{2k} (-1)^{2k-l} \binom{2k}{l} \times \left(\frac{\lambda_t}{2}\right)^{0.5(2k-l)} \int_{\sqrt{\frac{1}{2\lambda_t}}}^{y_{\mathrm{U}}} y^{l+0.5} \ln\left(2y^2\right) dy. \quad (99)$$

Using the logarithmic identities $\log(xy) = \log x + \log y$ and $\log(y^x) = x \log y$, $\mathcal{I}_{4b,3}$ can be written as (100) on page 20. Subsequently, with the aid of [77, Eq. 1.6.1.18, pp. 241], the second integral is solved and the final equation can be expressed as (101) on page 20.

REFERENCES

[1] D. Evans, "The internet of things: How the next evolution of the internet is changing everything," Cisco IBSG., US, Apr. 2011. [Online]. Available: https://www.cisco.com/c/dam/en_us/about/ac79/docs/innov/IoT_IBSG_0411FINAL.pdf

[2] M. A. Al-Jarrah, M. A. Yaseen, A. Al-Dweik, O. Dobre, and E. Alsusa, "Decision fusion for IoT-based wireless sensor networks," *IEEE Internet Things J.*, vol. 7, no. 2, pp. 1313-1326, Feb. 2020, doi: 10.1109/JIOT.2019.2954720.

[3] L. Chettri and R. Bera, "A comprehensive survey on internet of things (IoT) toward 5G wireless systems," *IEEE Internet Things J.*, vol. 7, no. 1, pp. 16-32, Jan. 2020, doi: 10.1109/JIOT.2019.2948888.

[4] L. Yang, R. Muresan, A. Al-Dweik and L. Hadjileontiadis, "Image-based visibility estimation algorithm for intelligent transportation systems," *IEEE Access*, vol. 6, pp. 76728-76740, 2018, doi: 10.1109/ACCESS.2018.2884225.

[5] M. Al-Jarrah, E. Alsusa, A. Al-Dweik and D. K. C. So, "Capacity analysis of IRS-based UAV communications with imperfect phase compensation," *IEEE Wireless Commun. Lett.*, vol. 10, no. 7, pp. 1479-1483, July 2021, doi: 10.1109/LWC.2021.3071059.

[6] M. Al-Jarrah, A. Al-Dweik, E. Alsusa, Y. Iraqi and M.-S. Alouini, "On the performance of IRS-assisted multi-layer UAV communications with imperfect phase compensation," *IEEE Trans. Commun.*, vol. 69, no. 12, pp. 8551-8568, Dec. 2021, doi: 10.1109/TCOMM.2021.3113008.

[7] F. Liu, C. Masouros, A. Li, and T. Ratnarajah, "Robust MIMO beamforming for cellular and radar coexistence," *IEEE Wireless Commun. Lett.*, vol. 6, no. 3, pp. 374-377, Jun. 2017.

[8] F. Liu, L. Zhou, C. Masouros, A. Li, W. Luo, and A. Petropulu, "Toward dual-functional radar-communication systems: Optimal waveform design," *IEEE Trans. Signal Process.*, vol. 66, no. 16, pp. 4264-4279, Aug. 2018.

[9] F. Liu, C. Masouros, A. Li, H. Sun, and L. Hanzo, "MU-MIMO communications with MIMO radar: From co-existence to joint transmission," *IEEE Trans. Wireless Commun.*, vol. 17, no. 4, pp. 2755-2770, Apr. 2018.

[10] A. Liu *et al.*, "A survey on fundamental limits of integrated sensing and communication," *IEEE Commun. Surveys Tuts.*, vol. 24, no. 2, pp. 994-1034, Secondquarter 2022, doi: 10.1109/COMST.2022.3149272.

[11] J. A. Zhang *et al.*, "An overview of signal processing techniques for joint communication and radar sensing," *IEEE J. Sel. Topics Signal Process*., vol. 15, no. 6, pp. 1295-1315, Nov. 2021, doi: 10.1109/JSTSP.2021.3113120.

[12] M. Temiz, E. Alsusa, and M. Baidas, "A dual-functional massive MIMO OFDM communication and radar transmitter architecture," *IEEE Trans. Veh. Technol.*, vol. 69, no. 12, pp. 14974-14988, Dec. 2020, doi: 10.1109/TVT.2020.3031686.

[13] M. Temiz, E. Alsusa and M. Baidas, "Optimized precoders for massive MIMO OFDM dual radar-communication systems," *IEEE Trans. Commun.*, vol. 69, no. 7, pp. 4781-4794, Jul. 2021, doi: 10.1109/TCOMM.2021.3068485.

[14] M. A. Al-Jarrah, A. Al-Dweik, S. Ikki, and E. Alsusa, "Spectrum-occupancy aware cooperative spectrum sensing using adaptive detection," *IEEE Systems J.*, vol. 14, no. 2, pp. 2225-2236, Jun. 2020, doi: 10.1109/JSYST.2019.2922773.

[15] S. Chen, H. Xu, D. Liu, B. Hu, and H. Wang, "A vision of IoT: Applications, challenges, and opportunities with china perspective," *IEEE Internet Things J.*, vol. 1, no. 4, pp. 349-359, Aug. 2014, doi: 10.1109/JIOT.2014.2337336.

[16] Mohammad A. Al-Jarrah, N. Al-Ababneh, M. Al-Ibrahim, and R. Al-Jarrah, "Cooperative OFDM for semi distributed detection in wireless sensor networks," *AEU-Int. J. of Electron. Commun.*, vol. 68, no. 10, pp. 1022-1029, 2014.

[17] L. Zhang, L. Zhang, and B. Du, "Deep learning for remote sensing data: A technical tutorial on the state of the art," *IEEE Geosci. Remote Sens. Mag.*, vol. 4, no. 2, pp. 22-40, Jun. 2016, doi: 10.1109/MGRS.2016.2540798.

[18] M. A. Al-Jarrah, A. Al-Dweik, E. Alsusa, and E. Damiani, "RFID reader localization using hard decisions with error concealment," *IEEE Sensors J.*, vol. 19, no. 17, pp. 7534-7542, Sep., 2019, doi: 10.1109/JSEN.2019.2914914.

[19] E. Fishler, A. Haimovich, R. Blum, L. Cimini, D. Chizhik, and R. Valenzuela, "Spatial diversity in radars—Models and detection performance," *IEEE Trans. Signal Process.*, vol. 54, no. 3, pp. 823-838, Mar. 2006.

[20] I. Bekkerman and J. Tabrikian, "Target detection and localization using MIMO radars and sonars," *IEEE Trans. Signal Process.*, vol. 54, no. 10, pp. 3873-3883, Oct. 2006, doi: 10.1109/TSP.2006.879267.

[21] A. Hassanien and S. Vorobyov, "Phased-MIMO radar: A tradeoff between phased-array and MIMO radars," *IEEE Trans.Signal Process.*, vol. 58, no. 6, pp. 3137-3151, Jun. 2010, doi: 10.1109/TSP.2010.2043976.

[22] H. Godrich, A. Haimovich, and R. Blum, "Target localization accuracy gain in MIMO radar-based systems," *IEEE Trans. Inf. Theory*, vol. 56, no. 6, pp. 2783-2803, Jun. 2010, doi: 10.1109/TIT.2010.2046246.

[23] B. Friedlander, "On transmit beamforming for MIMO radar," *IEEE Trans. Aerosp. Electron. Syst*., vol. 48, no. 4, pp. 3376-3388, Oct. 2012.

[24] N. Fatema, G. Hua, Y. Xiang, D. Peng, and I. Natgunanathan, "Massive MIMO linear precoding: A survey," *IEEE Sys. J.*, vol. 12, no. 4, pp. 3920-3931, Dec. 2018, doi: 10.1109/JSYST.2017.2776401.

[25] M. Shafi *et al.*, "5G: A tutorial overview of standards, trials, challenges, deployment, and practice," *IEEE J. Sel. Areas Commun.*, vol. 35, no. 6, pp. 1201-1221, Jun. 2017, doi: 10.1109/JSAC.2017.2692307.

[26] Samsung, "Massive MIMO for new radio," SAMSUNG, South Korea, Dec. 2020, [Online]. Available: https://images.samsung.com/is/content/samsung/assets/global/business/networks/insights/white-papers/1208_massive-mimo-for-new-radio/MassiveMIMOforNRTechnicalWhitePaper-v1.2.0.pdf

[27] ZTE, "5G massive MIMO network application," ZTE, China, Sep. 2020, [Online]. Available: https://res-www.zte.com.cn/mediares/zte/Files/PDF/white_book/202009101153.pdf

[28] J. Tang, N. Li, Y. Wu, and Y. Peng, "On detection performance of MIMO radar: A relative entropy-based study," *IEEE Signal Process. Lett.*, vol. 16, no. 3, pp. 184-187, Mar. 2009, doi: 10.1109/LSP.2008.2011704.

[29] B. Tang, J. Tang, and Y. Peng, "MIMO radar waveform design in colored noise based on information theory," *IEEE Trans. Signal Process.*, vol. 58, no. 9, pp. 4684-4697, Sep. 2010, doi: 10.1109/TSP.2010.2050885.

[30] T. M. Cover and J. A. Thomas, *Elements of Information Theory*. New York: Wiley, 1991.

[31] B. Tang, M. Naghsh, and J. Tang, "Relative entropy-based waveform design for MIMO radar detection in the presence of clutter and interference," *IEEE Trans. Signal Process.*, vol. 63, no. 14, pp. 3783-3796, Jul. 2015, doi: 10.1109/TSP.2015.2423257.

$$\mathcal{I}_{4b,3} = 4\left(2\right)^{-0.25}\exp\left(\frac{\lambda_t}{2}\right)\sum_{k=0}^{\infty}\frac{\left(-1\right)^k}{k!}\sum_{l=0}^{2k}\left(-1\right)^{2k-l}\binom{2k}{l}\left(\frac{\lambda_t}{2}\right)^{0.5(2k-l)}\left(\ln 2\int_{\sqrt{\frac{1}{2\lambda_t}}}^{y_{\mathrm{U}}} y^{l+0.5}dy + 2\int_{\sqrt{\frac{1}{2\lambda_t}}}^{y_{\mathrm{U}}} y^{l+0.5}\ln y dy\right). \quad (100)$$

$$\begin{aligned}\mathcal{I}_{4b,3} \;=\; & 4\left(2\right)^{-0.25}\exp\left(\frac{\lambda_t}{2}\right)\sum_{k=0}^{\infty}\frac{\left(-1\right)^k}{k!}\sum_{l=0}^{2k}\left(-1\right)^{2k-l}\binom{2k}{l}\left(\frac{\lambda_t}{2}\right)^{0.5(2k-l)}\left(\frac{\ln 2}{l+1.5}\left(\left(\sqrt{\frac{\lambda_t}{2}}+\frac{5}{\sqrt{2}}\right)^{l+1.5}-\left(\frac{1}{2\lambda_t}\right)^{\frac{l+1.5}{2}}\right)\right.\\ & \left.+2\left(y_{\mathrm{U}}^{l+1.5}\left(\frac{\ln\left(y_{\mathrm{U}}\right)}{l+1.5}-\frac{1}{\left(l+1.5\right)^2}\right)-\left(\frac{1}{2\lambda_t}\right)^{\frac{l+1.5}{2}}\left(\frac{-\ln\left(2\lambda_t\right)}{2\left(l+1.5\right)}-\frac{1}{\left(l+1.5\right)^2}\right)\right)\right). \quad (101)\end{aligned}$$

[32] M. Al-Jarrah, R. Al-Jarrah, N. Al-Ababneh, "Decision fusion in mobile wireless sensor networks using cooperative multiple symbol differential space time coding," *AEU-Int. J. Electron. Commun*., vol. 80, pp. 127-136, 2017.

[33] A. Khawar, A. Abdelhadi and C. Clancy, "Target detection performance of spectrum sharing MIMO radars," *IEEE Sensors J*., vol. 15, no. 9, pp. 4928-4940, Sep. 2015.

[34] J. Zuk, "Correlated noncoherent radar detection for gamma-fluctuating targets in compound clutter," *IEEE Trans. Aerosp. Electron. Syst*, vol. 58, no. 2, pp. 1241-1256, Apr. 2022, doi: 10.1109/TAES.2021.3113629.

[35] H. Li, F. Wang, C. Zeng, and M. Govoni, "Signal detection in distributed MIMO radar with non-orthogonal waveforms and sync errors," *IEEE Trans. Signal Process*., vol. 69, pp. 3671-3684, 2021, doi: 10.1109/TSP.2021.3087897.

[36] Z. Liu and A. Nehorai, "Statistical angular resolution limit for point sources," *IEEE Trans. Signal Process*., vol. 55, no. 11, pp. 5521-5527, Nov. 2007, doi: 10.1109/TSP.2007.898789.

[37] M. El Korso, R. Boyer, A. Renaux, and S. Marcos, "Statistical resolution limit for source localization with clutter interference in a MIMO radar context," *IEEE Trans. Signal Process.*, vol. 60, no. 2, pp. 987-992, Feb. 2012, doi: 10.1109/TSP.2011.2174232.

[38] A. Zaimbashi, "Forward M-ary hypothesis testing based detection approach for passive radar," *IEEE Trans. Signal Process.*, vol. 65, no. 10, pp. 2659-2671, 15 May 2017, doi: 10.1109/TSP.2017.2666778.

[39] L. Wang, W. Zhu, Y. Zhang, Q. Liao, and J. Tang, "Multi-target detection and adaptive waveform design for cognitive MIMO radar," *IEEE Sensors J*., vol. 18, no. 24, pp. 9962-9970, Dec. 2018, doi: 10.1109/JSEN.2018.2873103.

[40] W. Yi, T. Zhou, Y. Ai, and R. S. Blum, "Suboptimal low complexity joint multi-target detection and localization for non-coherent MIMO radar with widely separated antennas," *IEEE Trans. Signal Process.*, vol. 68, pp. 901-916, 2020, doi: 10.1109/TSP.2020.2968282.

[41] Y. Zhang, L. Wang, J. Tang, and J. Pan, "Multi-hypothesis test for close targets detection in co-located MIMO radar," *J. Eng.*, pp. 5986-5989, May 2019. Online. [Available:] https://doi.org/10.1049/joe.2019.0456.

[42] A. Chiriyath, B. Paul, and D. Bliss, "Radar-communications convergence: Coexistence, cooperation, and co-design," *IEEE Trans. Cogn. Commun. Netw.*, vol. 3, no. 1, pp. 1-12, Mar. 2017, doi: 10.1109/TCCN.2017.2666266.

[43] A. Chiriyath, B. Paul, G. Jacyna, and D. Bliss, "Inner bounds on performance of radar and communications co-existence," *IEEE Trans. Signal Process.*, vol. 64, no. 2, pp. 464-474, Jan. 2016, doi: 10.1109/TSP.2015.2483485.

[44] M. Temiz, E. Alsusa, and M. Baidas, "A dual-function massive MIMO uplink OFDM communication and radar architecture," *IEEE Trans. Cogn. Commun. Netw.*, vol. 8, no. 2, pp. 750-762, doi: 10.1109/TCCN.2021.3128599.

[45] P. Kumari, J. Choi, N. González-Prelcic, and R. Heath, "IEEE 802.11ad-based radar: An approach to joint vehicular communication-radar system," *IEEE Trans. Veh. Technol.*, vol. 67, no. 4, pp. 3012-3027, Apr. 2018, doi: 10.1109/TVT.2017.2774762.

[46] K. Singh, S. Biswas, T. Ratnarajah, and F. Khan, "Transceiver design and power allocation for full-duplex MIMO communication systems with spectrum sharing radar," *IEEE Trans. Cogn. Commun. Netw.*, vol. 4, no. 3, pp. 556-566, Sep. 2018, doi: 10.1109/TCCN.2018.2830758.

[47] X. Yuan *et al.*, "Spatio-temporal power optimization for MIMO joint communication and radio sensing systems with training overhead," *IEEE Trans. Veh. Technol.*, vol. 70, no. 1, pp. 514-528, Jan. 2021, doi: 10.1109/TVT.2020.3046438.

[48] C. Xu, B. Clerckx, S. Chen, Y. Mao, and J. Zhang, "Rate-splitting multiple access for multi-antenna joint communication and radar transmissions," *2020 IEEE Int. Conf. Commun. Workshops (ICC Workshops)*, Dublin, Ireland, 2020, pp. 1-6, doi: 10.1109/ICCWorkshops49005.2020.9145168.

[49] N. Luong, X. Lu, D. Hoang, D. Niyato, and D. Kim, "Radio resource management in joint radar and communication: A comprehensive survey," *IEEE Commun. Surveys Tuts.*, vol. 23, no. 2, pp. 780-814, Secondquarter 2021, doi: 10.1109/COMST.2021.3070399.

[50] B. Chalise, M. Amin, and B. Himed, "Performance tradeoff in a unified passive radar and communications system," *IEEE Signal Process. Lett.*, vol. 24, no. 9, pp. 1275-1279, Sep. 2017, doi: 10.1109/LSP.2017.2721639.

[51] C.-C Ouyang, Y. Liu, and H. Yang, "Performance of downlink and uplink integrated sensing and communications (ISAC) systems," *IEEE Wireless Commun. Lett.*, vol. 11, no. 9, pp. 1850-1854, Sep. 2022, doi: 10.1109/LWC.2022.3184409.

[52] C.-C. Ouyang, Y. Liu, and H. Yang, "On the performance of uplink ISAC systems," *IEEE Commun. Lett.*, vol. 26, no. 8, pp. 1769-1773, Aug. 2022, doi: 10.1109/LCOMM.2022.3178193.

[53] Z. Xiao and Y. Zeng, "Waveform design and performance analysis for full-duplex integrated sensing and communication," *IEEE J. Sel. Areas Commun.*, vol. 40, no. 6, pp. 1823-1837, Jun. 2022, doi: 10.1109/JSAC.2022.3155509.

[54] L. Gaudio, M. Kobayashi, B. Bissinger, and G. Caire, "Performance analysis of joint radar and communication using OFDM and OTFS," *2019 IEEE Int. Conf. Commun. Workshops (ICC Workshops)*, 2019, pp. 1-6, doi: 10.1109/ICCW.2019.8757044.

[55] M. Ahmadipour, M. Kobayashi, M. Wigger, and G. Caire, "An information-theoretic approach to joint sensing and communication," *IEEE Trans. Inf. Theory*, IEEE early access, 2022, doi: 10.1109/TIT.2022.3176139.

[56] Z. Yun and M. F. Iskander, "Ray tracing for radio propagation modeling: Principles and applications," *IEEE Access*, vol. 3, pp. 1089-1100, 2015, doi: 10.1109/ACCESS.2015.2453991.

[57] R. Feng, E. D. Greef, M. Rykunov, H. Sahli, S. Pollin and A. Bourdoux, "Multipath ghost recognition for indoor MIMO radar," *IEEE Trans. Geosci. Remote Sens.*, vol. 60, Art no. 5104610, pp. 1-10, 2022, doi: 10.1109/TGRS.2021.3109381

[58] J. Chen, S. Guo, H. Luo, N. Li and G. Cui, "Non-line-of-sight multi-target localization algorithm for driver-assistance radar system," *IEEE Trans. Veh. Technology.*, IEEE early access, 2022, doi: 10.1109/TVT.2022.3227971.

[59] S. Kullback, *Information Theory and Statistics*. Dover Publications, NY, USA, 1978.

[60] K. Burnham and D. Anderson, *Model selection and Multimodel Inference: A Practical Information-Theoretic Approach*. Springer-Verlang, USA, 2002.

[61] W. Press, S. Teukolsky, W. Vetterling and B. Flannery, *Numerical Recipes: The Art of Scientific Computing*, 3rd Edition. Cambridge University Press, USA, 2007.

[62] C. Bishop, *Pattern Recognition and Machine Learning*. Springer-Verlang, USA, 2006.

[63] A. Stavridis, M. Renzo, and H. Haas, "Performance analysis of multi-stream receive spatial modulation in the MIMO broadcast channel," *IEEE*

Trans. Wireless Commun., vol. 15, no. 3, pp. 1808-1820, Mar. 2016, doi: 10.1109/TWC.2015.2496597.

[64] A. Goldsmith, *Wireless Communications*. Cambridge University Press, 2005.

[65] A. Prudnikov, Y. Brychkov, and O. Marichev, *Integrals Series: Special Functions*, 3rd ed. London, U.K.: Gordon and Breach Science Publishers, 1986.

[66] H. Zhang, B. Zong, and J. Xie, "Power and bandwidth allocation for multi-target tracking in collocated MIMO radar," *IEEE Trans. Veh. Technol.*, vol. 69, no. 9, pp. 9795-9806, Sep. 2020, doi: 10.1109/TVT.2020.3002899.

[67] H. Zhang, J. Shi, Q. Zhang, B. Zong, and J. Xie, "Antenna selection for target tracking in collocated MIMO radar," *IEEE Trans. Aerosp. Electron. Sys.*, vol. 57, no. 1, pp. 423-436, Feb. 2021, doi: 10.1109/TAES.2020.3031767.

[68] A. Hassanien and S. Vorobyov, "Transmit energy focusing for DOA estimation in MIMO radar with colocated antennas," *IEEE Trans. Signal Process.*, vol. 59, no. 6, pp. 2669-2682, Jun. 2011, doi: 10.1109/TSP.2011.2125960.

[69] H. Xu, J. Wang, J. Yuan, and X. Shan, "Colocated MIMO radar transmit beamspace design for randomly present target detection," *IEEE Signal Process. Lett.*, vol. 22, no. 7, pp. 828-832, Jul. 2015, doi: 10.1109/LSP.2014.2371241.

[70] H. Xu, R. S. Blum, J. Wang, and J. Yuan, "Colocated MIMO radar waveform design for transmit beampattern formation," *IEEE Trans. Aerosp. Electron. Sys.*, vol. 51, no. 2, pp. 1558-1568, Apr. 2015, doi: 10.1109/TAES.2014.140249.

[71] K. Sayana, J. Zhuang and K. Stewart, IEEE 802.16 Broadband Wireless Access Working Group: Channel Estimation Modeling for System Simulations. Technical Report, no. IEEE C802.16m-07/208, Motorola Inc 600, N US Hwy 45, Libertyville, IL, 2007.

[72] P. Arvidson, Channel Estimation Error Model for SRS in LTE. Technical Report, nO. EAB/FJL-10:0537 Uen, Ericsson, 2010.

[73] S. Kay, *Fundementals of Statistical Signal Processing: Part II*. Englewood Cliffs, NJ: Prentice-Hall, 1998.

[74] M. Abramowitz and I. Stegun, *Handbook of Mathematical Functions with Formulas*, New York, 1972.

[75] I. Gradshteyn and I. Ryzhik, *Table of Integrals, Series and Products*, 7th ed. USA: Academic Press, 2000.

[76] D. Hinkley, "On the ratio of two correlated normal random variables," *Biometrika*, vol. 56, no. 3, pp. 635–639, Dec. 1969, doi:10.2307/2334671. JSTOR 2334671.

[77] Prudnikov, Y. Brychkov, and O. Marichev, *Integrals Series: Elementary Functions*. 3rd ed. London, U.K.: Gordon and Breach Science Publishers, 1986.

BIOGRAPHIES

Mohammad Al-Jarrah (Member, IEEE) received the B.Sc. and M.S. degrees in electrical engineering/wireless communications from Jordan University of Science and Technology (JUST), Irbid, Jordan, in 2008 and 2011, respectively. He is currently working toward his Ph.D. degree in electrical and electronics engineering at the The University of Manchester, Manchester, U.K.

From 2017 to 2019, he had been working as a Lab Instructor with Khalifa University (KU), Abu Dhabi, United Arab Emirates. Currently, he is a Marie Curie Early Stage Researcher with the Department of Electrical and Electronic Engineering, The University of Manchester, UK. His research interests include distributed decision fusion systems, statistical signal processing, target tracking in wireless sensor networks, RFID communications, cooperative spectrum sensing, integrated radar and communications, IRS systems, and backhauling and cellular planning for future cellular networks.

Emad Alsusa (M'06–SM'07) received the Ph.D. degree in electrical and electronic engineering from the University of Bath, Bath, U.K., in 2000. He then joined the University of Edinburgh, Edinburgh, U.K., as a Mobile VCE Postdoctoral Research Fellow, working on link enhancement techniques for future high-data-rate wireless communication systems. In 2003, he joined The University of Manchester, Manchester, U.K., as an academic member of the School of Electrical and Electronic Engineering, where he lectures on communication engineering. His research interests include signal processing techniques and the analysis of wireless communication networks, with particular focus on cognitive radio, interference mitigation, multiuser multiple-input multiple-output, green communications, and energy and spectrum optimization techniques. Dr. Alsusa has served as a Technical Program Committee Member for numerous IEEE flagship conferences and chaired the Manchester EEE postgraduate conference in 2010.

Christos Masouros (Senior Member, IEEE) received the Diploma degree in Electrical and Computer Engineering from the University of Patras, Greece, in 2004, and MSc by research and PhD in Electrical and Electronic Engineering from the University of Manchester, UK in 2006 and 2009 respectively. In 2008 he was a research intern at Philips Research Labs, UK, working on the LTE standards. Between 2009-2010 he was a Research Associate in the University of Manchester and between 2010-2012 a Research Fellow in Queen's University Belfast. In 2012 he joined University College London as a Lecturer. He has held a Royal Academy of Engineering Research Fellowship between 2011-2016.

Since 2019 he is a Full Professor of Signal Processing and Wireless Communications in the Information and Communication Engineering research group, Dept. Electrical and Electronic Engineering, and affiliated with the Institute for Communications and Connected Systems, University College London. His research interests lie in the field of wireless communications and signal processing with particular focus on Green Communications, Large Scale Antenna Systems, Integrated Sensing and Communications, interference mitigation techniques for MIMO and multicarrier communications. Between 2018-22 he was the Project Coordinator of the €4.2m EU H2020 ITN project PAINLESS, involving 12 EU partner universities and industries, towards energy-autonomous networks. Between 2024-28 he will be the Scientific Coordinator of the €2.7m EU H2020 DN project ISLANDS, involving 19 EU partner universities and industries, towards next generation vehicular networks. He was the recipient of the 2023 IEEE ComSoc Stephen O. Rice Prize, co-recipient of the 2021 IEEE SPS Young Author Best Paper Award and the recipient of the Best Paper Awards in the IEEE GlobeCom 2015 and IEEE WCNC 2019 conferences. He has been recognised as an Exemplary Editor for the IEEE Communications Letters, and as an Exemplary Reviewer for the IEEE Transactions on Communications. He is an Editor for IEEE Transactions on Wireless Communications, the IEEE Open Journal of Signal Processing, and Editor-at-Large for IEEE Open Journal of the Communications Society. He has been an Editor for IEEE Transactions on Communications, IEEE Communications Letters, and a Guest Editor for a number of IEEE Journal on Selected Topics in Signal Processing and IEEE Journal on Selected Areas in Communications issues. He is a founding member and Vice-Chair of the IEEE Emerging Technology Initiative on Integrated Sensing and Communications (SAC), Vice Chair of the IEEE Wireless Communications Technical Committee Special Interest Group on ISAC, and Chair of the IEEE Green Communications Computing Technical Committee, Special Interest Group on Green ISAC. He is the TPC chair for the IEEE ICC 2024 Selected Areas in Communications (SAC) Track on ISAC.